NSG-5258

DETERMINATION OF TROPICAL CYCLONE SURFACE PRESSURE AND WINDS FROM SATELLITE MICROWAVE DATA

BY
STANLEY Q. KIDDER

Atmospheric Scienc

PAPER NO.

307

US ISSN 0067-0340

DEPARTMENT OF ATMOSPHERIC SCIENCE
COLORADO STATE UNIVERSITY
FORT COLLINS, COLORADO

DETERMINATION OF TROPICAL CYCLONE SURFACE PRESSURE AND WINDS FROM SATELLITE MICROWAVE DATA

by

Stanley Q. Kidder

Department of Atmospheric Science

Colorado State University

Fort Collins, Colorado

April, 1979

Atmospheric Science Paper No. 307

ABSTRACT

A new approach to the problem of deducing wind speed and pressure around tropical cyclones is presented. The technique, called the Surface Wind Inference from Microwave data (SWIM) technique, uses satellite microwave sounder data to measure upper tropospheric temperature anomalies which may then be related to surface pressure anomalies through the hydrostatic and radiative transfer equations. Although current satellite instruments have too coarse resolution to accurately estimate central pressure, surface pressure gradients outside of the radius of maximum wind are estimated for the first time. Future instruments may be able to estimate central pressure with $\pm$ 0.1 kPa accuracy.

Surface pressure gradients determined by the SWIM technique are related to surface wind speeds using the gradient wind equation and a shearing parameter. The method is first tested using simulated satellite data constructed from temperature, pressure, and height data recorded by aircraft reconnaissance of four hurricanes. Wind speeds in the 80-95 kPa region are estimated with 2-3 m s^{-1} accuracy. Next, data from the 55.45 GHz channel of the Nimbus 6 Scanning Microwave Spectometer (SCAMS) over eight typhoons during 1975 are used to estimate the radii of 15.4 m s^{-1} (30 kt) and 25.7 m s^{-1} (50 kt) winds. Accuracies of $\pm$ 80 km and $\pm$ 65 km, respectively, were found. These results are sufficient to provide valuable information to forecasters. It is suggested that the technique be further tested using data from the 54.96 GHz channel of the TIROS-N Microwave Sounding Unit (MSU) launched in October, 1978.

ACKNOWLEDGMENTS

This paper constitutes the author's Ph.D. dissertation which could not have been completed without the help of many people. The author would first like to thank his advisor, Dr. Thomas H. Vonder Haar, for his support and encouragement along the way. Thanks are also due to Dr. William Gray for his enthusiasm and for the use of his tropical cyclone rawinsonde data set, and to the rest of the author's committee, Drs. Stephen K. Cox and David A. Krueger, for useful comments and suggestions. The author is indebted to Drs. David H. Staelin and Phil W. Rosenkranz of MIT for their help in interpretting the SCAMS data tapes; to LCDR David Sokol of the Joint Typhoon Warning Center and Mr. Samson Brand of the Naval Environmental Prediction Research Facility for supplying data on the typohoons of 1975; to Dr. Hans J. Liebe of the U.S. Department of Commerce Office of Telecommunications for a computer subroutine to compute atmospheric absorption coefficients; and to Dr. William M. Frank, formerly of CSU, for helpful discussions. This research was sponsored by the National Aeronautics and Space Administration under grant NSG-5258.

TABLE OF CONTENTS

LIST OF TABLES

LIST OF FIGURES

LIST OF FIGURES (continued)

1.0 INTRODUCTION

Aircraft reconnaissance flights into tropical cyclones have long been the standard method of measuring surface wind speeds and central pressure. There are several disadvantages to this technique, however. The flights are expensive and are becoming less frequent, the spatial and temporal resolutions of the observations are low, and only the United States maintains a fleet of reconnaissance aircraft. It is becoming increasingly important, therefore, to monitor storms using satellite data. Scientists have been attempting to do this for many years beginning with Sadler (1964) and progressing through Fett (1966), Fritz et al. (1966), Dvorak (1975) and others. Today the scheme of Dvorak (1975) is widely used (Gaby et al., 1977) to estimate storm intensity (maximum sustained surface wind speed) and central pressure (minimum sea level pressure).

Although the Dvorak scheme is fairly accurate (6-10 m s^{-1} rms), three criticisms may be made. First it has a statistical rather than a physical basis. The forecaster classifies each storm according to categories based on various cloud characteristics, observed in visible or infrared satellite images, such as the nature and amount of banding, the shape of the cirrus overcast, and the appearance of the eye of the storm. These categories are statistically related to central pressure and maximum wind speed. It takes a significant amount of skill, acquired primarily by experience, to correctly classify a storm. Second, Arnold (1977) has shown that convection is not well related to storm intensity; thus the Dvorak technique probably cannot be improved by using higher resolution data. And third, the Dvorak scheme does not estimate winds at outer radii, which are not well related to maximum

wind speed or to central pressure. Outer wind speed is important for ship routing and disaster preparedness. Jelesniansky and Taylor (1973), for example, found that the shape of the wind profile is more important for storm surge prediction than maximum wind speed or central pressure.

More recently, geosynchronous satellite data have been used quite successfully to measure wind speeds around tropical storms by tracking low level clouds (Rodgers et al., 1977). While good accuracy has been achieved, the method has some drawbacks: it needs sophisticated man-interactive equipment to track the clouds; it is tedious to perform; and it requires the presence of trackable clouds. It cannot be executed in clear areas nor in areas obscured by high or middle level clouds (though low level clouds can sometimes be tracked through thin cirrus).

An attempt has previously been made to use microwave data to infer tropical cyclone winds. Rosenkranz et al. (1978) have used data from the 22.235 GHz and 31.65 GHz channels of the Nimbus 6 Scanning Microwave Spectrometer (SCAMS) to infer surface wind speeds in the central core of Typhoon June of 1975. Their technique requires the assumption that the atmosphere is saturated; thus it is useful only in the inner core.

The research reported in this paper explores a new approach to the problem of surface wind speed determination from satellite data around tropical cyclones. We call the technique Surface Wind Inference from Microwave data (SWIM). It is an objective technique which is soundly based on the radiative transfer, hydrostatic, and gradient wind equations. In short, the tropical cyclone's upper level temperature anomaly is sensed using an upper tropospheric channel from a microwave sounder (such as the SCAMS 55.45 GHz channel). Brightness temperature anomalies are related to surface pressure anomalies through the radiative

transfer and hydrostatic equations. Surface winds at outer radii are then deduced from surface pressure gradients through the gradient wind equation. Because the microwave data are not significantly affected by clouds or precipitation, the SWIM technique can be used regardless of cloud cover. A relatively small amount of data is used in the calculations; thus computing time is minimal.

A by-product of the SWIM technique is the estimation of surface pressure anomalies. The resolution of current microwave sounders is too coarse to allow accurate determination of central pressure or maximum wind speed, but improvements in future instruments may make such determinations possible.

Finally, it should be noted that it may be possible to use the SWIM technique in conjunction with other techniques to obtain a more complete view of the surface winds around tropical cyclones.

The SWIM technique will be presented after discussions of the interaction of microwave radiation with atmospheric constituents and of the temperature structure of tropical cyclones, which form the bases of the theory.

2.0 RADIATIVE TRANSFER THEORY

The SWIM technique depends on the determination of the magnitude of upper tropospheric temperature anomalies above tropical cyclones. This chapter reviews basic radiative transfer theory and details the method by which atmospheric temperatures may be inferred from satellite-borne, passive radiometers.

2.1 Basic Theory

The propagation of electromagnetic radiation through an atmosphere in local thermodynamic equilibrium is described by the radiative transfer equation (Chandrasekhar, 1960):

$$\frac{dL_\lambda}{ds} = -\sigma_e L_\lambda(\vec{r},\Omega_s) + \sigma_a B_\lambda(T)$$

$$+ \frac{\sigma_s}{4\pi} \int_0^{4\pi} \xi(\vec{r},\Omega_i,\Omega_s) L_\lambda(\vec{r},\Omega_i) d\Omega_i, \quad * \qquad (1)$$

where L_λ is the spectral radiance (power per unit wavelength per steradian per unit area perpendicular to Ω_s) at the point $\vec{r}$ in the direction Ω_s, $B_\lambda(T)$ is the Planck function, σ_s, σ_a, and σ_e ($\sigma_e \equiv \sigma_a + \sigma_s$) are the volume scattering, absorption and extinction coefficients, respectively, $\xi(\vec{r}, \Omega_i, \Omega_s)$ is the scattering phase function, and s is the distance along the ray path. Due to the local thermodynamic equilibrium condition, inelastic scattering need not be included (Goody, 1964). Qualitatively, Eq. (1) gives the rate of change of the radiance along the path at point $\vec{r}$ in the direction Ω_s in terms of 1) the radiance absorbed and scattered out of the beam by the

*Symbols and units in this paper conform to recommended usage by the International Association of Meteorology and Atmospheric Physics (IAMAP) Radiation Commission (1978).

atmosphere, 2) the radiance added to the beam by the thermal emission of the atmosphere, and 3) radiation scattered into the beam from other directions. In the microwave region ($\lambda > 1$ mm), the Planck function,

$$B_\lambda(T) = 2hc^2\lambda^{-5}(e^{hc/\lambda kT}-1)^{-1}, \tag{2}$$

where h is Planck's constant, c speed of light, k Boltzmann's constant, and T thermodynamic temperature, can be replaced with the Rayleigh-Jeans approximation. In this region at temperatures observed in the atmosphere, $hc/\lambda kT << 1$. Therefore,

$$B_\lambda(T) = 2kc\lambda^{-4}T. \tag{3}$$

If Eq. (1) is multiplied by $\lambda^4(2kc)^{-1}$,

$$\frac{dT_B}{ds} = -\sigma_e T_B(\vec{r},\Omega_s) + \sigma_a T + \frac{\sigma_s}{4\pi}\int_0^{4\pi} \xi(\vec{r},\Omega_i,\Omega_s)T_B(\vec{r},\Omega_i)d\Omega_i . \tag{4}$$

The quantity $T_B \equiv \lambda^4(2kc)^{-1} L_\lambda$ is called the brightness temperature because it is equal to the temperature of a black body emitting spectral radiance L_λ*. T_B, like L_λ, is a conservative quantity; that is, it does not vary as the inverse square of the distance from an object in a vacuum.

The brightness temperature measured by a satellite-borne radiometer can be obtained by integrating the first-order, linear differential Eq. (4) from the earth's surface to the top of the

*The factor $\lambda^4(2kc)^{-1}$ has units m^3W^{-1} K sr, that is it has an additional unit sr so that T_B has the unit K instead of K sr^{-1}.

atmosphere, H. At this point it is customary to invoke plane-parallel geometry (Figure 1) in which atmospheric temperature, absorption and scattering coefficients, and scattering phase function are functions of height (z) only. While this geometry is not exactly appropriate for the problem studied in this research (the temperature in a tropical cyclone is definitely a function of radius), the equations will be developed using plane-parallel geometry, and it will be shown in Section 3.3 that the results are independent of geometry. Performing the above-mentioned integration, yields,

$$T_B(\theta) = T_{B_o}(\theta)\, \tau_{o,H}^{\sec\theta} + \int_0^H \tau_{z,H}^{\sec\theta} \, [\sigma_a T(z) + \sigma_s S_c] \sec\theta \, dz, \qquad (5)$$

where

$$S_c \equiv \frac{1}{4\pi} \int_0^{4\pi} \xi(\vec{r}, \Omega_i, \Omega_s) T_B(r, \Omega_i) d\Omega_i \, . \qquad (6)$$

The vertical transmittance between heights a and b is

$$\tau_{a,b} \equiv e^{-\delta_{a,b}} , \qquad (7)$$

where $\delta_{a,b}$ is the optical depth,

$$\delta_{a,b} = \int_a^b \sigma_e \, dz \, . \qquad (8)$$

The surface brightness temperature, T_{B_o}, consists of two terms, the radiation emitted by and reflected by the surface:

$$T_{B_o} = \varepsilon(\theta) T_s + T_{B_R} , \qquad (9)$$

where $\varepsilon(\theta)$ is the surface emittance, T_s is the thermodynamic surface temperature, and T_{B_R} is the reflected sky brightness temperature. For a specular surface,

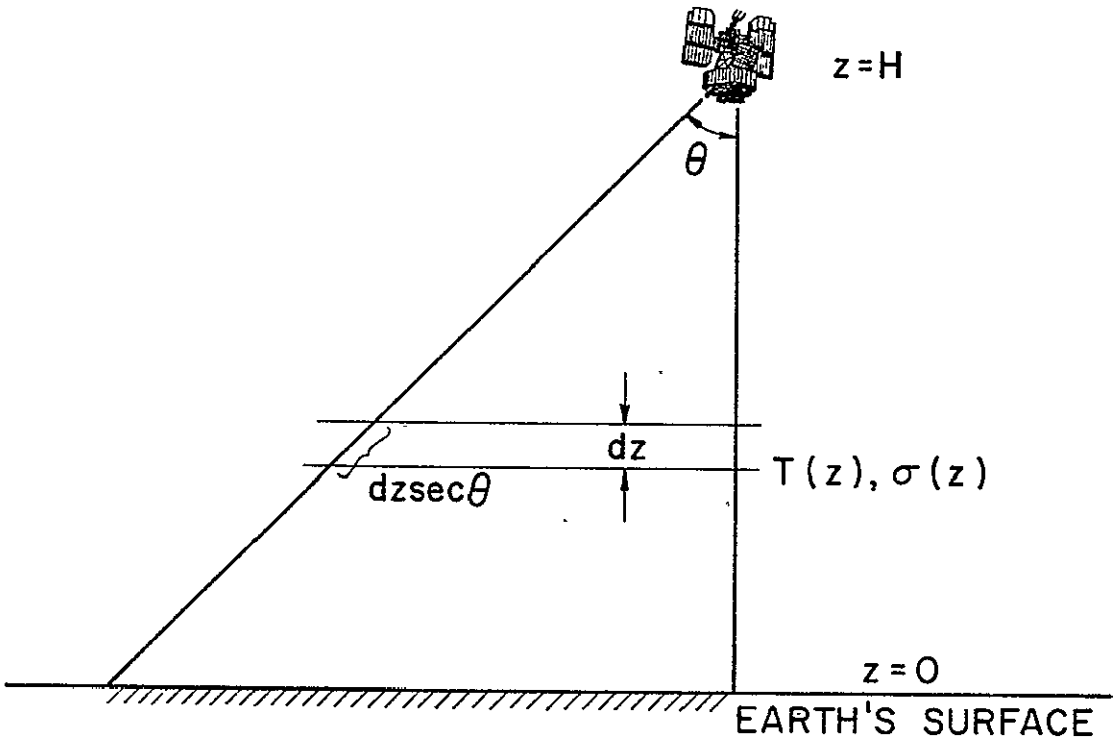

Figure 1. Plane-parallel geometry

$$T_{B_R}(\theta) = [1 - \varepsilon(\theta)]T_{B_{sky}}(\theta) \ , \tag{10}$$

where $T_{B_{sky}}$ is the sky brightness temperature. The brightness temperature measured by the satellite, then, can be rewritten

$$T_B(\theta) = [\varepsilon(\theta)T_s + T_{B_R}]\ \tau_{o,H}^{\sec\theta} + \int_0^H \tau_{z,H}^{\sec\theta}\ [\sigma_a T(z) + \sigma_s S_c]\sec\theta\ dz \ . \tag{11}$$

Qualitatively, Eq. (8) gives the brightness temperature measured by the satellite as the sum of 1) that portion of the apparent surface brightness temperature which is transmitted through the atmosphere, and 2) the energy which is emitted and scattered into the beam along the atmospheric path and then transmitted to the satellite.

2.2 Active Atmospheric Constituents

The three atmospheric constituents which significantly affect the transfer of microwave radiation are oxygen (O_2), water vapor, and liquid water (Westwater, 1972). Trace constituents such as ozone and carbon monoxide have absorption lines in the microwave region, but because they are not plentiful enough to affect electromagnetic radiation at the frequencies used in this research, they will not be discussed further. Figure 2 shows the calculated transmittance of the 15° North Annual Atmosphere (U.S. Standard Atmosphere Supplements, 1966). Trace gasses have been neglected. The absorption lines at 22.235 GHz and 183.31 GHz are water vapor rotational transitions caused by the interaction of electromagnetic radiation with the H_2O electric dipole moment (Van Vleck, 1947a). The band near 60 GHz (actually numerous overlapping lines) and the line at 118.75 GHz have been described as "spin reorientation"

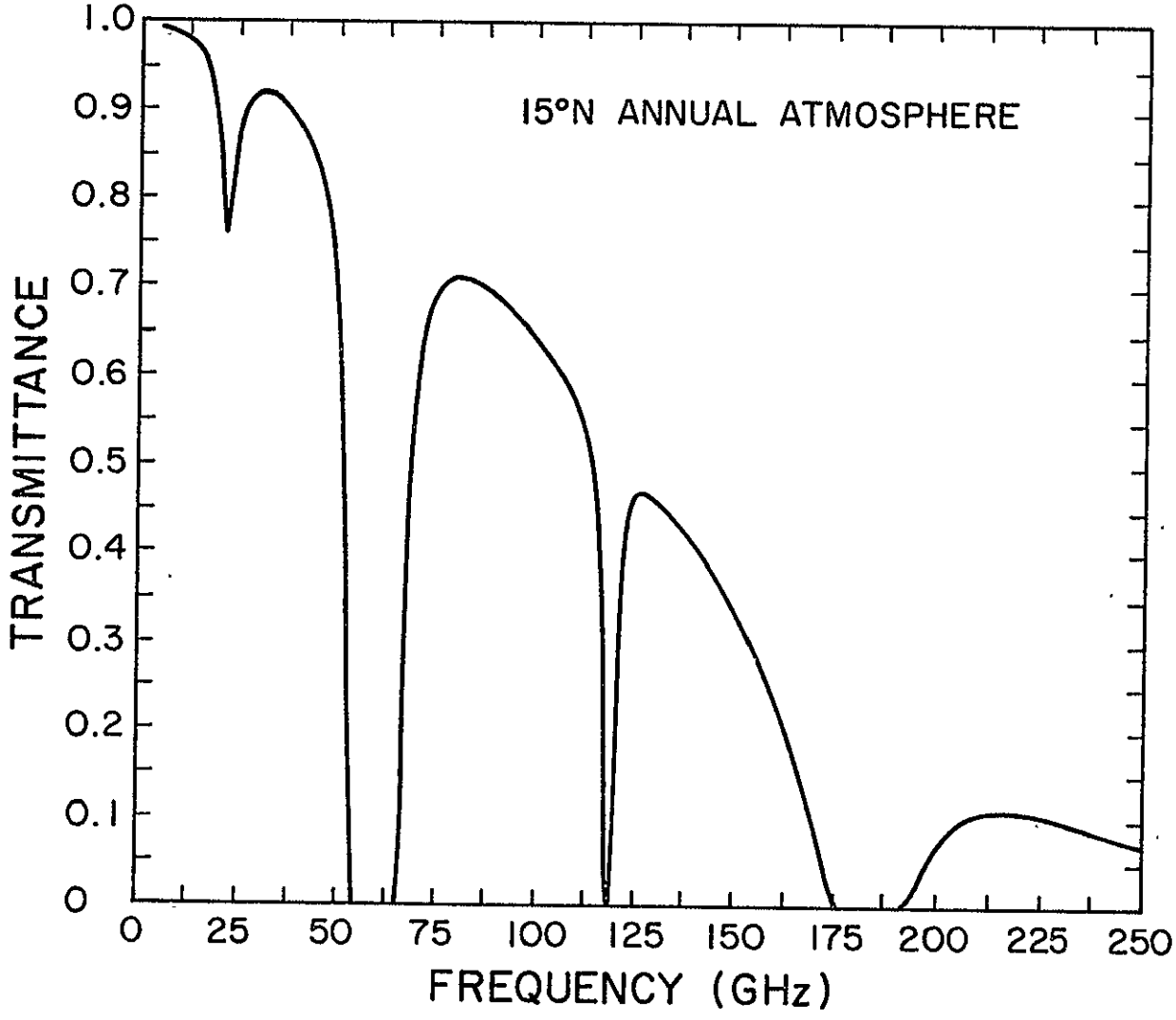

Figure 2. Transmittance of the 15° North Annual Atmosphere

transitions (Herzberg, 1950); electromagnetic radiation interacts with the oxygen molecule's magnetic dipole moment to change the molecule's spin (Van Vleck, 1947b).

All of the gaseous absorption coefficients used in this study were calculated with a computer algorithm supplied to the author by Dr. Hans J. Liebe.* The algorithm was first described in Liebe et al. (1977) and was revised in Liebe and Gimmestad (1978). The algorithm was modified slightly to be useful above 35 km where pressure broadening has decreased to the point that Doppler broadening and Zeeman splitting are important. This modification was accomplished using Eq. (11) from Liebe and Gimmestad (1978) with a value of 0.35×10^{-4} Tesla for H (the earth's magnetic field strength); this value represents a coarse average for the tropics (Chapman and Bartels, 1962). The algorithm uses Rosenkranz's (1975) pressure-broadened line shape model modified by a set of interference coefficients to produce good agreement between theory and observations of the microwave spectrum in moist air. The absorption coefficient, which includes both oxygen and water vapor absorption, is calculated as a function of frequency (range: 10-300 GHz), temperature (175-310 K), dry air pressure (0.01-101 kPa), and water vapor pressure (0-6 kPa). The calculated absorption coefficients agree with observations to within the 4% experimental uncertainties of the observations (Liebe and Gimmestad, 1978).

Atmospheric liquid water may be divided into two classes: Cloud-size drops and precipitation-size drops (Deirmendjian, 1963).

*Institute of Telecommunication Sciences, Office of Telecommunications, U.S. Dept. of Commerce, Boulder, CO 80302.

In clouds with modal drop radius less than 50 μm (which includes the vast majority of clouds (Fletcher, 1963)), the scattering of microwave radiation with frequencies less than 60 GHz may be neglected in comparison with absorption. Clouds, therefore may be treated with a simple absorption coefficient which is proportional to the cloud liquid water content (Westwater, 1972). Figure 3 shows the volume cloud absorption coefficient for a 0°C cloud normalized to a liquid water content of 1 g m^{-3}. Using a typical value of vertically integrated liquid water content for a nonprecipitating cloud (0.2 kg m^{-2}), one can quickly estimate from Figure 3 that typical nonprecipitating clouds have optical depths of approximately 0.1 and thus transmittances of about 90% near 60 GHz. This is the greatest advantage of remote sensing in the microwave region: clouds are essentially transparent to microwave radiation. Figure 3 also shows that microwave absorption for ice clouds is approximately two orders of magnitude less than for water clouds. Calculations of cloud absorption coefficients made in this research all used the formula of Westwater (1972). A more complete analysis of the effects of clouds and precipitation on the SWIM technique will be presented later.

Water droplets which are large enough to have significant fall velocities (to precipitate) are large enough to interact strongly with microwave radiation. Scattering, therefore, cannot be neglected in precipitating layers, and to obtain a complete understanding of the transfer of microwave radiation through these layers, one must use the full Mie equations (Deirmendjian, 1963). These calculations are lengthy and complicated, but a few things can be said in general.

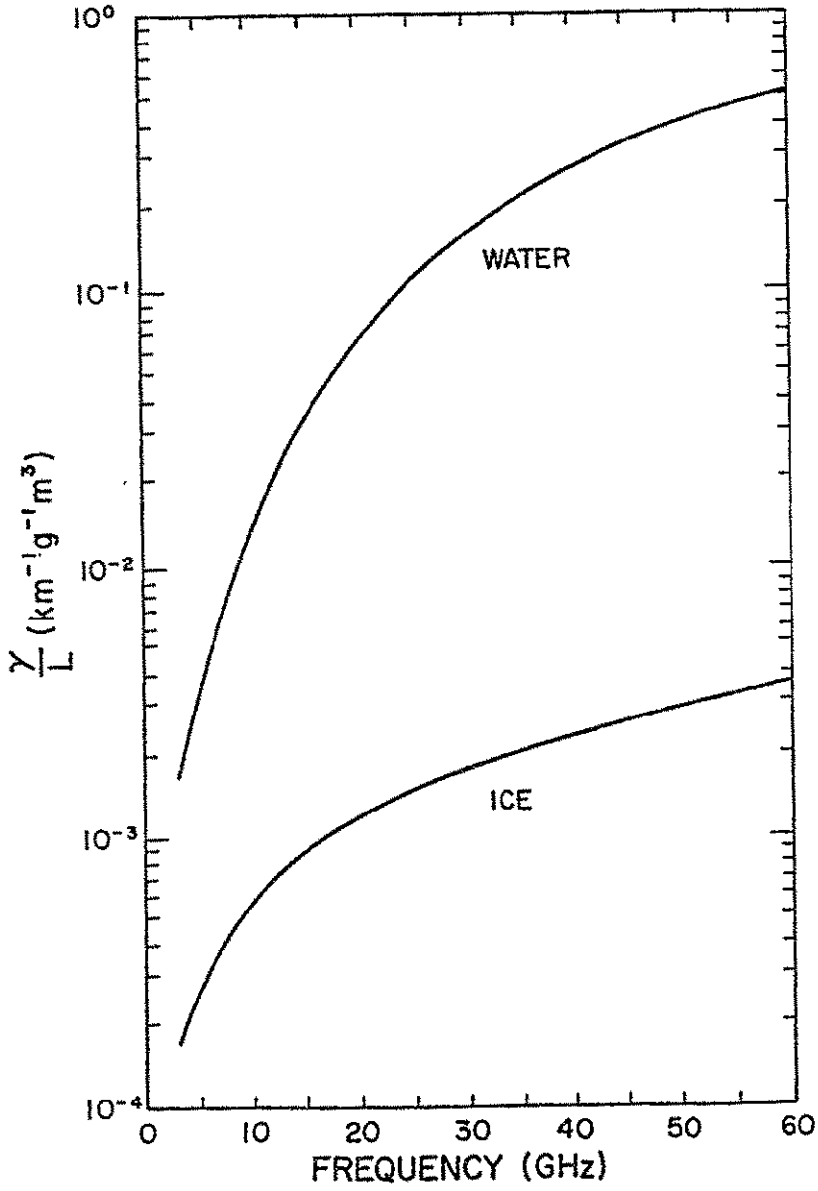

Figure 3. Cloud absorption coefficient (γ) per unit liquid water content (L) (after Westwater, 1972).

First, because the complex index of refraction of ice is much less than that of water (1.78-0.0024i and 4.75-2.77i, respectively, at 24.2 GHz and 0°C) ice particles interact much less strongly with microwave radiation than water particles (Battan, 1973). In fact most microwave models used in remote sensing ignore frozen precipitation completely, though this may not be completely valid (Savage, 1976).

Second, for frequencies below about 50 GHz, the atmosphere, even with clouds, is very transparent to microwave radiation. Adding precipitation-size particles increases the opacity of the column. Over the land, which has a high background brightness temperature (see next section), the increased opacity causes the cooler atmosphere to be more evident, and the satellite observed brightness temperature tends to fall. Over the ocean, which has a low background brightness temperature, precipitation tends to increase the brightness temperature to a point where backscattering becomes important. For precipitation rates higher than this saturation precipitation rate, the brightness temperature decreases (see Figure 4). As frequency increases, this saturation point occurs at lower precipitation rates.

Finally, as frequency approaches the center of an absorption band such as the 60 GHz O_2 band, the radiation sensed by a satellite comes from increasingly higher levels in the atmosphere (see Section 2.4). Because the density of precipitation, especially nonfrozen precipitation, decreases with height, it has a decreasing effect on satellite-measured brightness temperature as the frequency approaches the band center. The effects of precipitation will be further discussed in Section 2.4.

2.3 Surface Characteristics

Because the atmosphere is so transparent through much of the microwave spectrum, surface characteristics become important. Three

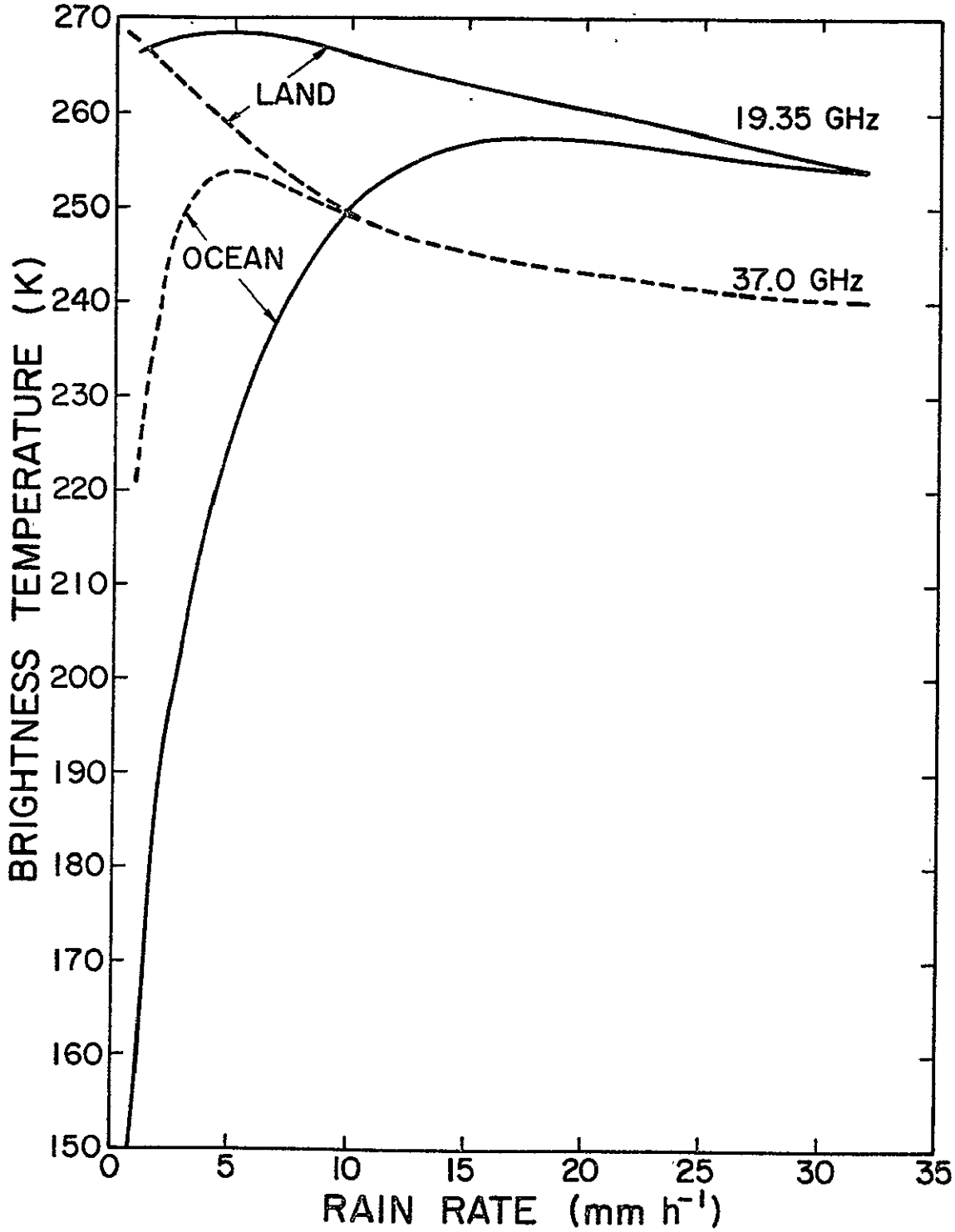

Figure 4. Satellite-observed brightness temperatures as functions of rain rate for different backgrounds (after Savage, 1976)

types of surfaces are common: ocean, land, and ice. Land emittance depends on soil type, vegetation, and moisture content, and ice emittance depends on the age of the ice, but both are near 0.9 (Wilheit, 1972). The emittance of the ocean surface is more important for this work. For a plane water surface, the emittance can be calculated from electromagnetic theory (see Kidder, 1976). Figure 5 shows the emittance of a smooth ocean surface (for nadir viewing) as a function of frequency and surface temperature. Figure 6 shows the variation of emittance as a function of viewing angle. The dielectric constant of the ocean was calculated according to Stogryn (1971) using a 3.5% by weight NaCl solution.

The ocean surface is very seldom smooth, however. Wind causes waves of many scales, and the emittance of the sea surface changes with wind speed. Stogryn (1967) has modelled this effect. Figures 7-8 show the 19.4 GHz brightness temperature of a 290 K ocean as a function of viewing angle and wind speed. For nadir viewing, wind speed (at least low wind speeds) make very little difference in emittance, but at higher viewing angles, wind speed increases emittance. Figure 8 shows that brightness temperature increases approximately linearly with wind speed at a viewing angle of 50° (with some variation due to the direction of the wind with respect to the plane of observation).

At wind speeds higher than 7 m s^{-1}, foam begins to form on the sea surface, and the brightness temperature increases. In an aircraft experiment over the North Atlantic, Nordberg et al. (1971) found that the 19.35 GHz nadir brightness temperature increased linearly with wind speeds greater than 7 m s^{-1}. Because the sea surface temperature

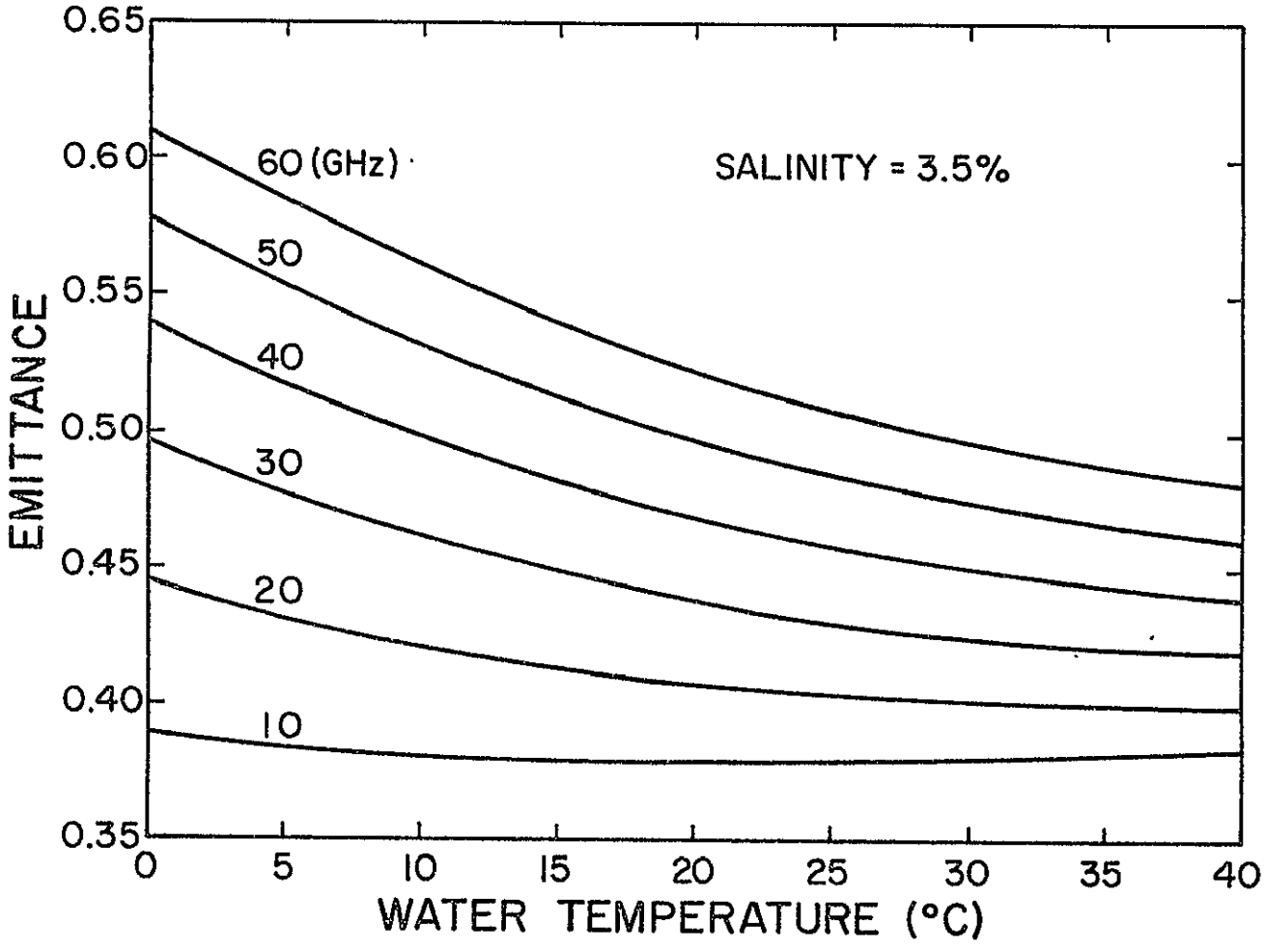

Figure 5. Nadir emittance of a smooth ocean surface as a function of surface temperature

on these flights ranged from 275 K to 283 K, this brightness temperature increase translates to an emittance increase of 4.3×10^{-3} m^{-1} s for wind speeds greater than 7 m s^{-1}.

The above relationships indicate that one should be able to determine surface wind speeds over the ocean from satellite microwave data; however, corrections must be made for competing effects such as water vapor, cloud liquid water, and precipitation. The solution is to use a multichannel radiometer to simultaneously solve for all of these variables. Such a radiometer, the Scanning Multichannel Microwave Radiometer (SMMR), was launched on the Nimbus-7 satellite (October 24, 1978).

2.4 Retrieving Atmospheric Temperature Profiles

Multichannel microwave radiometers operating in the 5 mm oxygen band may be used analogously to infrared radiometers operating in the 15 μm CO_2 band to produce atmospheric temperature profiles (soundings). The advantage of microwave sounders is that they see through clouds. The theoretical basis for remotely sounding the atmosphere is outlined below.

If scattering is neglected and if Eq. (10) is used for the reflection term, we have

$$T_B(\theta) = \left[\varepsilon(\theta)\, T_s + [1-\varepsilon(\theta)] T_{B_{sky}}\right] \tau_{o,H}^{\sec\theta} + \int_0^H \tau_{z,H}^{\sec\theta}\, \sigma_a \sec\theta\, T(z)\, dz \,. \qquad (12)$$

In a plane parallel atmosphere $T_{B_{sky}}(\theta)$ is given by

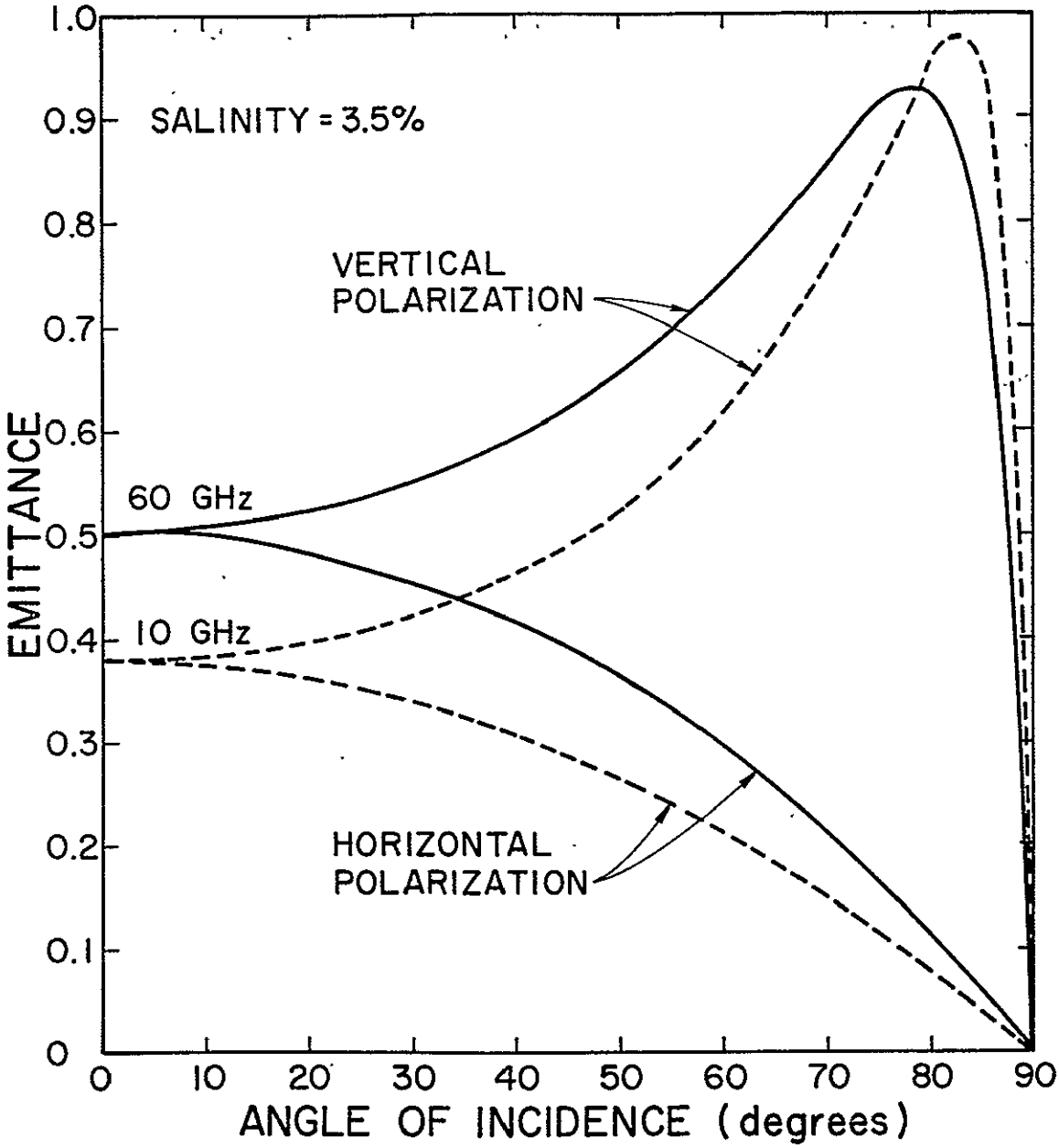

Figure 6. Emittance of a smooth ocean surface as a function of zenith angle

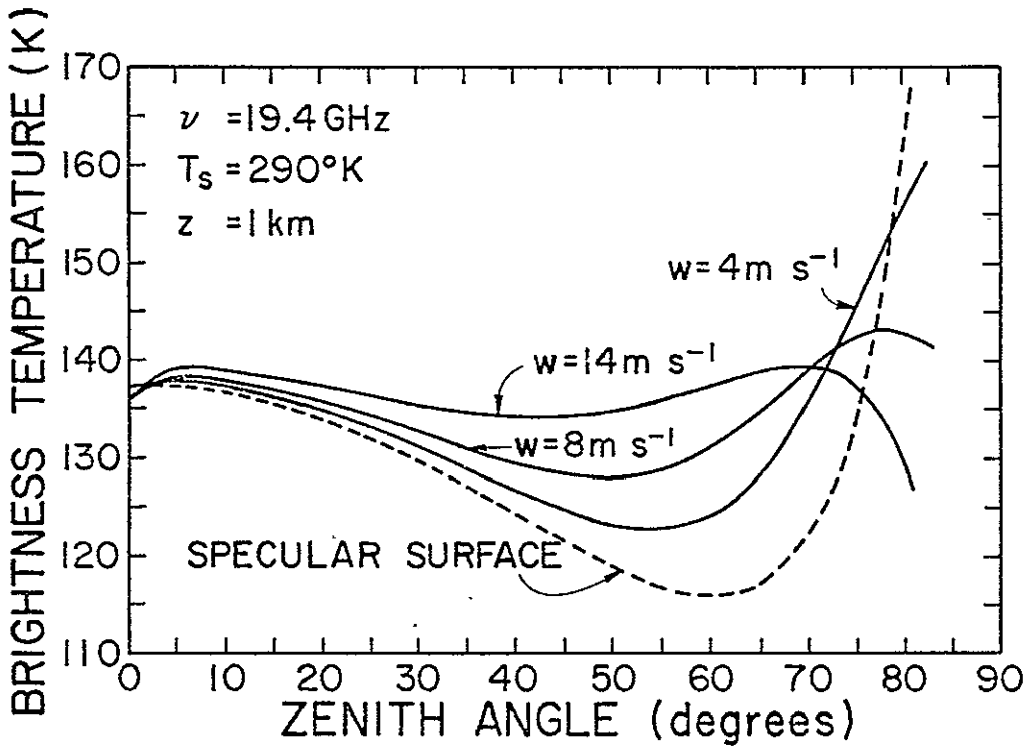

Figure 7. 19.4 GHz brightness temperature of the ocean surface as a function of zenith angle at a height of 1 km for several wind speeds (after Stogryn, 1967)

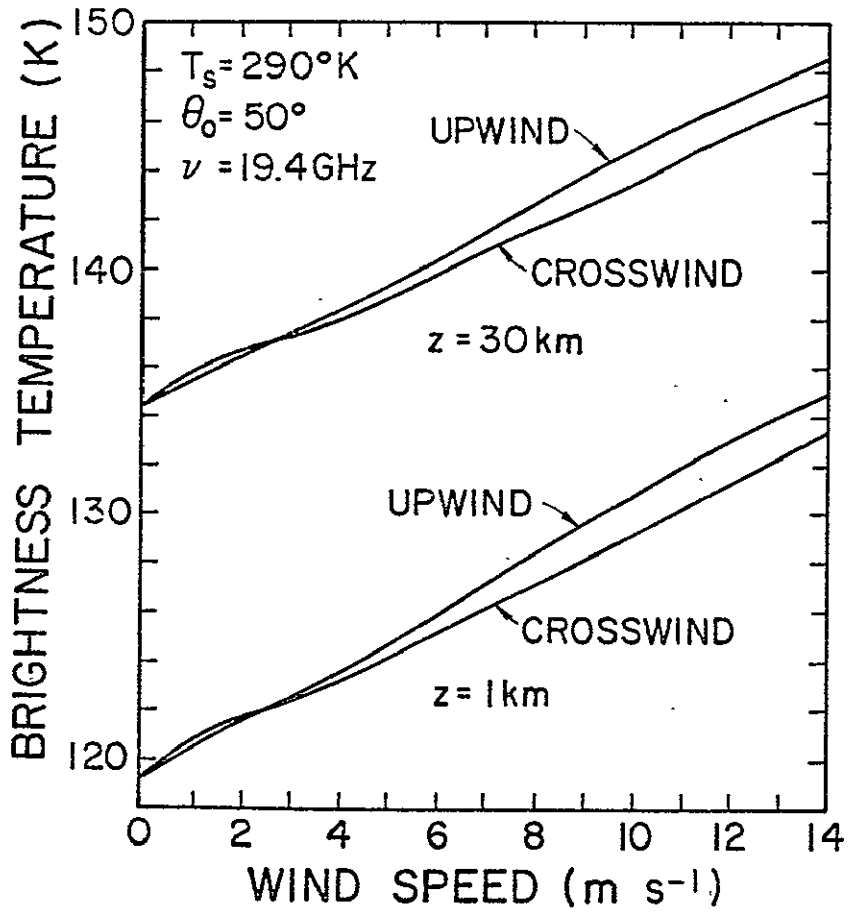

Figure 8. 19.4 GHz brightness temperature of the ocean surface as a function of wind speed for a zenith angle of 50° (after Stogryn, 1967)

$$T_{B_{sky}}(\theta) = \int_0^H T(z)\sigma_a \sec\theta \, \tau_{o,z}^{\sec\theta} \, dz \tag{13}$$

Therefore,

$$T_B(\theta) = \varepsilon(\theta)T_s\tau_{o,H}^{\sec\theta} + \int_0^H \left\{ \tau_{z,H}^{\sec\theta} + [1-\varepsilon(\theta)]\tau_{o,H}^{\sec\theta} \, \tau_{o,z}^{\sec\theta} \right\} \sec\theta\sigma_a T(z)dz \tag{14}$$

Noting that

$$\frac{d}{dz}\left(\tau_{z,H}^{\sec\theta}\right) = \sec\theta\sigma_a \, \tau_{z,H}^{\sec\theta} \, , \tag{15}$$

and that

$$\tau_{o,H} = \tau_{o,z} \, \tau_{z,H} \, , \tag{16}$$

we have

$$T_B(\theta) = \varepsilon(\theta)T_s\tau_{o,H}^{\sec\theta} + \int_0^H W_\lambda(\theta,z)T(z)dz \, , \tag{17}$$

where

$$W_\lambda(\theta,z) = \left\{ 1 + [1-\varepsilon(\theta)]\left(\frac{\tau_{o,H}}{\tau_{z,H}} \right)^{2\sec\theta} \right\} \frac{d}{dz}\left(\tau_{z,H}^{\sec\theta}\right) \, . \tag{18}$$

W_λ varies slowly with temperature and ε and more rapidly with viewing angle. Plots of the weighting functions (W_λ's) for the Nimbus 6 SCAMS and for the Microwave Sounding Unit (MSU) on board TIROS-N are shown in Figures 9-10. The 15° North Annual Atmosphere was used to calculate the weighting functions, but the U.S. Standard Atmosphere gives almost identical curves.

Because the weighting functions for different frequencies peak at different levels in the atmosphere, simultaneous measurements at several frequencies can be inverted to yield an atmospheric temperature sounding. Several methods are available to invert the sounding data (Fritz et al., 1972), but none of them will be discussed here. Because in a tropical cyclone standard assumptions about atmospheric structure

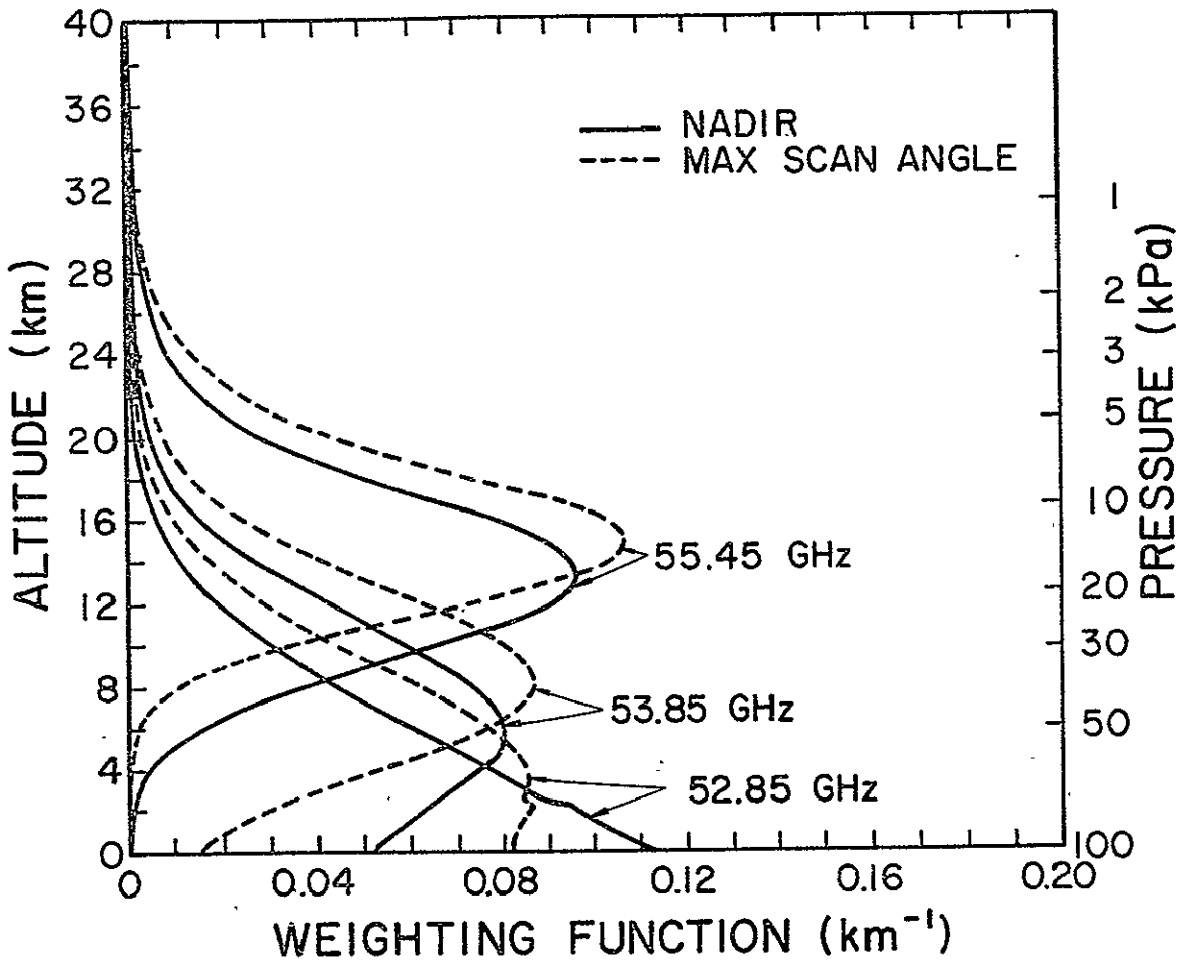

Figure 9. Weighting functions for the Nimbus 6 Scanning Microwave Spectrometer (SCAMS) in the 15° North Annual Atmosphere

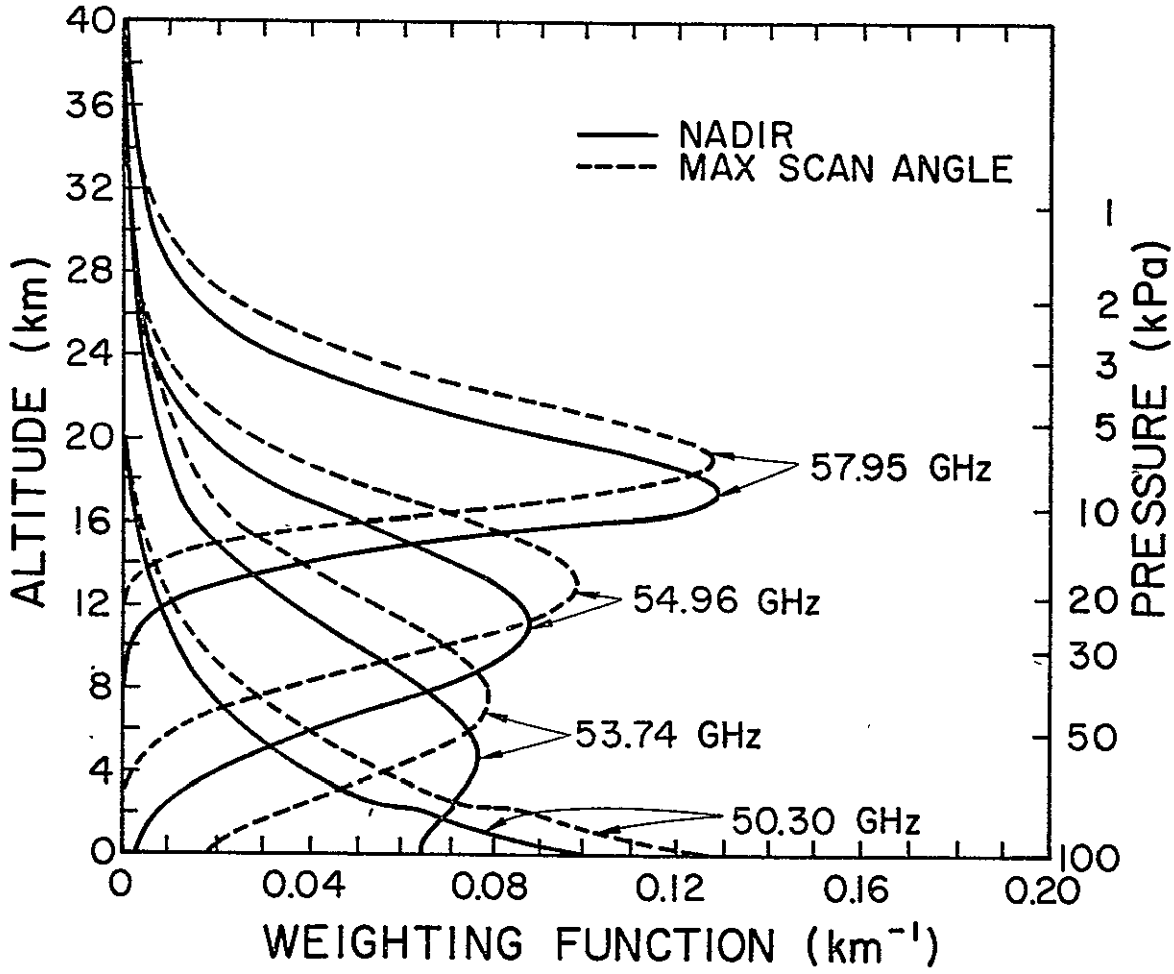

Figure 10. Weighting functions for the TIROS-N Microwave Sounding Unit (MSU) in the 15° North Annual Atmosphere

are not necessarily valid (see Section 3.1) and because high winds cause extensive foam formation on the ocean surface, normal inversion techniques do not work well. In this study, no use was made of inverted atmospheric soundings. Instead the brightness temperatures measured by the 55.45 GHz SCAMS channel were used directly. As can be seen in Figure 9, the 55.45 GHz brightness temperature is proportional to a weighted average upper tropospheric temperature; thus it can be used directly as a measure of the magnitude of the upper tropospheric warming above tropical cyclones.

The effects of clouds and precipitation on microwave radiation at frequencies used for sounding the atmosphere are important to this study and were closely examined. To estimate the magnitude of the cloud problem, a numerical computer model which performs the integration of Eq. (17) for externally prescribed atmospheric conditions was developed. The vertical resolution of the model was 0.5 km from the surface to 50 km. To avoid integration over the 220 MHz band width of the radiometer, the concept of an equivalent frequency was used (Waters, et al., 1975). Using the clear 15° North Annual Atmosphere over a smooth 300 K ocean, a frequency within the radiometer band width was found for each channel such that the nadir brightness temperature at that frequency was equal to the average brightness temperature over the band width of the radiometer. The equivalent frequencies so calculated are listed in Table 1.

The effects of clouds were assessed as follows. The 15° North Annual atmosphere was used as the basic atmosphere, and clouds of varying thicknesses were inserted at levels listed in Table 2. At the

Table 1

Equivalent Frequencies for the Nimbus 6

SCAMS and the TIROS-N MSU

Instrument	Center Frequency (GHz)	Equivalent Frequency (GHz)
SCAMS	55.450	55.491
SCAMS	53.850	53.868
SCAMS	52.850	52.837
MSU	57.950	57.876
MSU	54.960	54.978
MSU	53.740	53.666
MSU	50.300	50.301

Table 2

Model Cloud Properties

Cloud Type	Liquid Water Content ($g\ m^{-3}$)	Cloud Base (km)
Stratus	0.25	0
Altostratus	0.14	3
Cirrus	0.03(ice)	9

levels where clouds were inserted, the relative humidity was increased to 100%. The simulated brightness temperatures for the five SCAMS frequencies for various thicknesses of cloud over a 300 K ocean are listed in Table 3.

Several significant deductions may be made from the data in Table 3. First, cirrus clouds barely affect the brightness temperatures at all, and the small change in the lowest two channels is caused mostly by the increased water vapor. Second, the brightness temperature of the lowest two channels increase with increasing integrated liquid water and water vapor. However, channel 1, which is at the center of a water vapor rotation line, is more sensitive to water vapor than channel 2; channel 2, which is at a higher frequency than channel 1, is more sensitive to clouds. Third, the change in the brightness temperatures of channels 3 and 4 depend on the level at which the clouds are placed. Finally, and most important for this study, clouds have almost no effect on channel 5.

The effect rain has on microwave radiation in the 5 mm oxygen band is more difficult to assess. To date, no adequate scattering model calculations in the oxygen band have been reported. The difficulty is that atmospheric absorption in the oxygen band changes rapidly with height (by an order of magnitude) in the troposphere. Most scattering models consider a layer of raindrops with uniform properties, including gaseous absorption, throughout. Fortunately, however, the effect of rain on sounding channels can be empirically determined.

Shown in Figure 11 are the 11.5 μm imagery recorded by the Nimbus 6 Temperature Humidity Infrared Radiometer (THIR) and a plot of the

Table 3

Simulated Brightness Temperatures (K) for Different Cloud Conditions

Cloud Type	Thickness (km)	Integrated Liquid Water (mg cm^{-2})	Integrated Water Vapor (g cm^{-2})	Frequency (GHz) 22.235 (Ch.1)	31.65 (Ch.2)	52.85 (Ch.3)	53.85 (Ch.4)	55.45 (Ch.5)
No Clouds	--	0.0	3.92	189.95	152.79	260.80	255.81	219.12
Cirrus	1	4.0	3.96	190.67	152.84	260.79	255.80	219.12
Cirrus	2	7.0	3.97	190.94	152.87	260.79	255.80	219.12
Altostratus	1	18.7	4.60	200.97	161.81	262.26	255.72	219.10
Altostratus	2	32.7	4.90	206.60	168.14	262.94	255.49	219.10
Stratus	1	29.2	4.51	198.68	164.00	263.28	256.01	219.11
Stratus	2	54.2	4.86	204.84	172.85	264.93	256.08	219.10
All	2	93.8	5.89	219.43	185.92	266.00	255.66	219.07

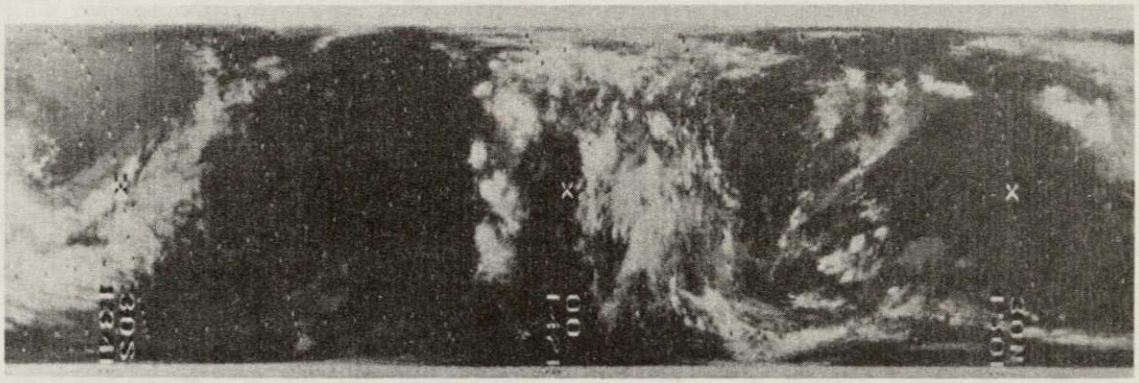

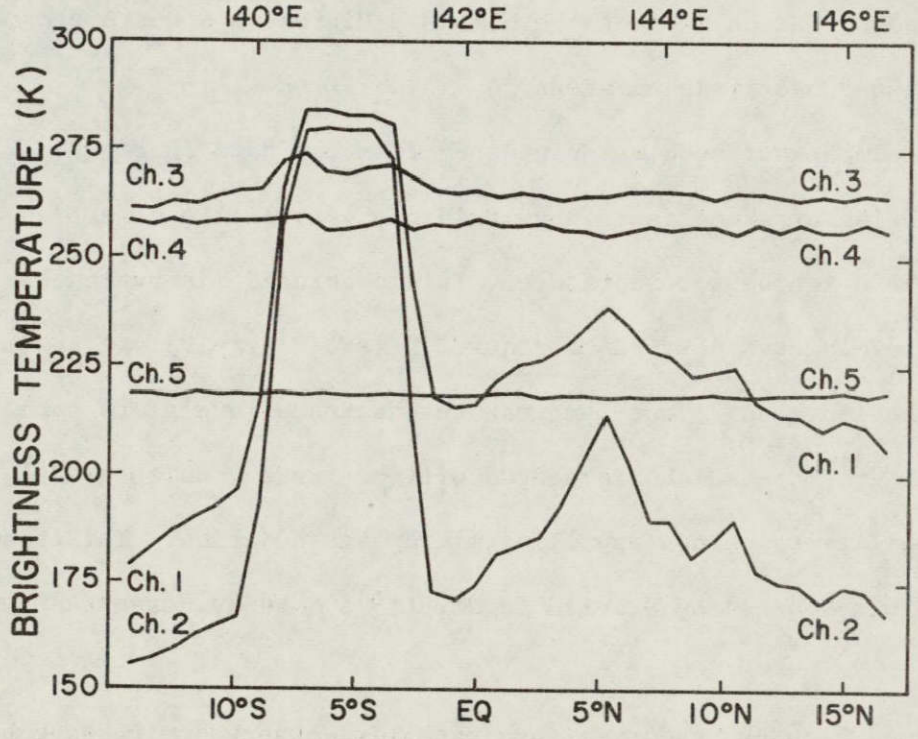

Figure 11. Data recorded by Nimbus-6 on 26 September 1975 on the descending portion of data orbit 1425; Top: 11.5 μm Temperature Humidity Infrared Radiometer (THIR) imagery; Bottom: Nadir brightness temperatures from the Scanning Microwave Spectrometer (SCAMS)

nadir brightness temperatures recorded by the Nimbus 6 SCAMS on September 26, 1975 on the descending portion of orbit 1425. The satellite passed directly over a large cloud cluster centered at about 5° North and then over New Guinea (under the cloud at 5° South). The brightness temperatures recorded by SCAMS channels 1 and 2 over the center of the cloud cluster (238.7 K and 214.0 K, respectively) are much larger than those calculated for the thickest clouds in Table 3 (219.4 K and 185.9 K, respectively), which indicates that rain is being detected. A further indication of rain is the small dip in the channel 4 brightness temperature; a similar dip was noted by Staelin et al. (1975) in the 53.65 GHz channel of the Nimbus E Microwave Spectrometer (NEMS) as it passed over raining areas.

The important conclusion reached from the data in Figure 11 and several similar examples is that rain has very little effect on the channel 5 brightness temperature. This conclusion is reasonable because 1) the levels sensed by SCAMS channel 5 (see Figure 9) are above most precipitation, and 2) the temperatures at those levels are cold enough that any droplets which are sensed will be frozen, which greatly reduces their ability to change upwelling microwave radiation. This same conclusion was reached by Staelin et al. (1975) and by Rosenkranz et al. (1978).

Armed with the theory of how satellite-observed microwave brightness temperature is related to the vertical temperature profile of the atmosphere, we are now ready to see how surface winds and pressures around tropical cyclones can be deduced.

3.0 DETERMINATION OF THE SURFACE PRESSURE FIELD

To obtain surface pressure information from satellite data, one must have knowledge of atmospheric temperature structure. In this chapter the temperature structure of tropical cyclones is discussed and an equation is derived which relates satellite-observed brightness temperature anomalies to surface pressure anomalies.

3.1 Tropical Cyclone Temperature Structure

The surface pressure drop in the center of a tropical cyclone is caused by warming in the upper troposphere (Frank, 1977). Núñez and Gray (1977) have calculated the mean temperature anomalies (differences from mean environmental temperature) in typhoons and in hurricanes from composited rawinsonde data. The anomalies as functions of pressure and distance from the storm center (radius) are tabulated in Appendix I and plotted in Figure 12. The main feature of the temperature anomaly profiles is a large warming centered between 25 kPa and 30 kPa and extending several hundred kilometers from the storm center.

The temperature anomaly profiles are remarkably similar in the two oceans, but there are differences. Atlantic storms are generally lower and less intense than Western Pacific storms; in Figure 12 the peak temperature anomalies are smaller in magnitude in the Atlantic and they occur lower in the atmosphere. Because there were few statistically significant anomalies in Atlantic storms below 70 kPa (see Appendix I), the anomaly profiles were extrapolated to zero at 70 kPa. Similarly for West Pacific storms the data were extrapolated to zero at 100 kPa. Above tropical cyclones there is a region which is cooler than the environment caused probably by evaporation of overshooting cloud tops

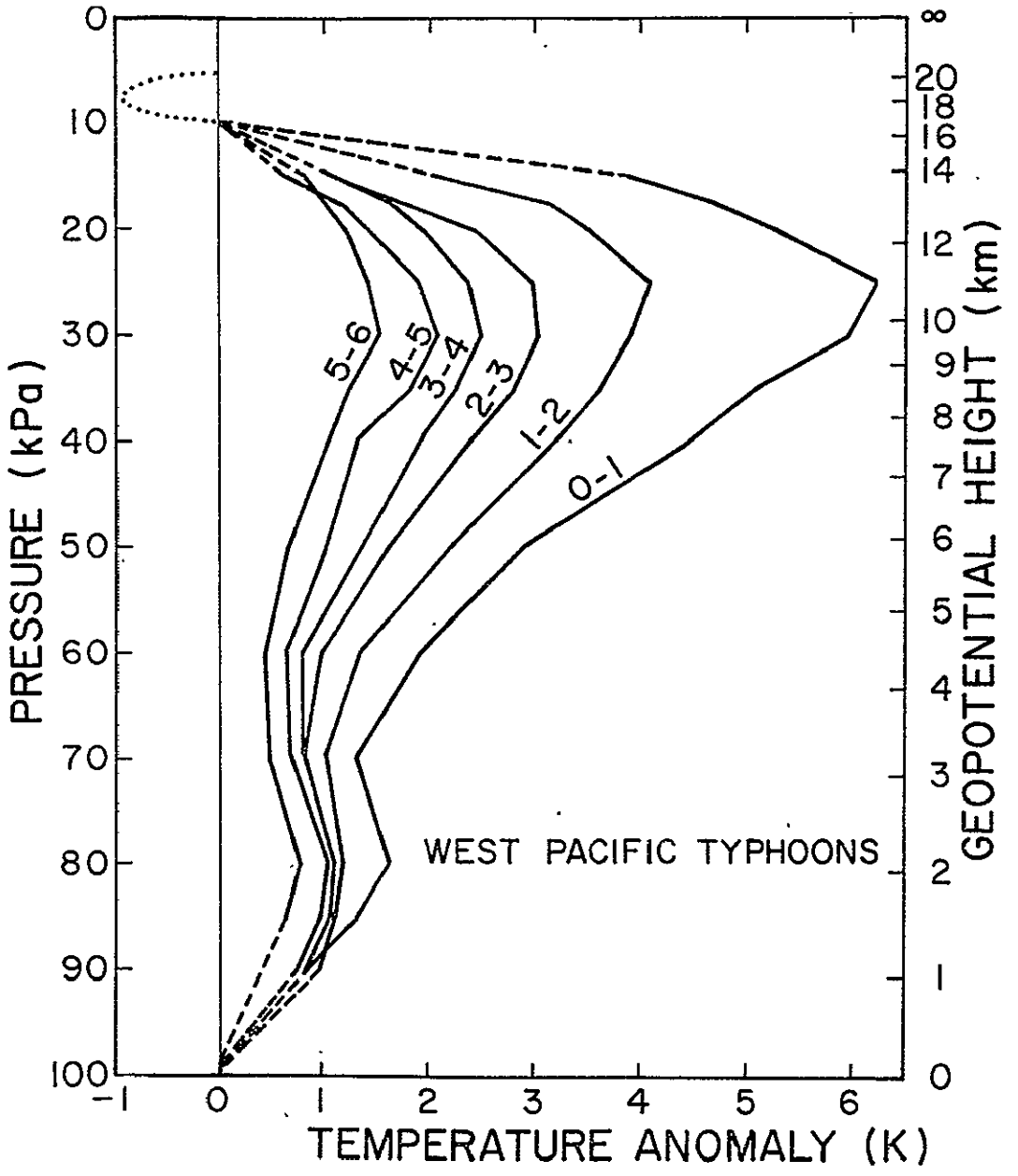

Figure 12a. Mean temperature anomalies in 1° radial bands for West Pacific typhoons (after Núñez and Gray, 1977)

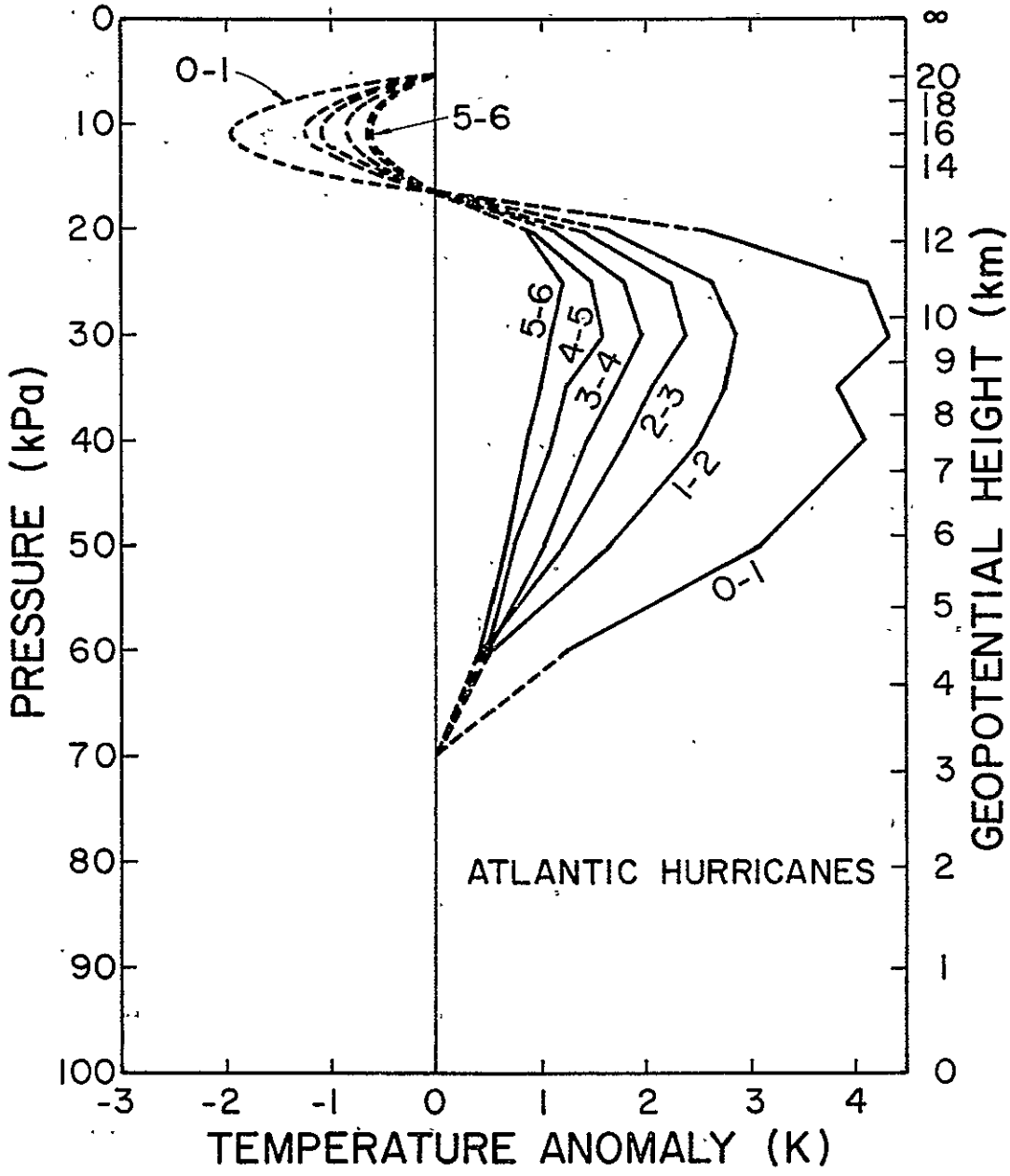

Figure 12b. Mean temperature anomalies in 1° bands for Atlantic (West Indies) hurricanes (after Núñez and Gray, 1977)

and/or radiative cooling of the top of the cirrus deck. For Atlantic storms the cooling was parameterized by assuming that above 20 kPa the temperature anomalies go to zero at 16.25 kPa and 5 kPa. Between these levels the cooling was assumed to be parabolic with the amplitude determined from the 20 kPa anomaly such that the slope was continuous across 16.25 kPa. This approximation gives a reasonable fit to the data in Appendix I. In the West Pacific, all of the cooling (shown schematically with the dotted line) appears above 10 kPa where it is difficult to make good rawinsonde observations. Because few statistically significant data points were available above 10 kPa, and because it made an insignificant difference in the final calculations, the temperature anomalies in the West Pacific were assumed to go to zero at 10 kPa, and cooling above this level was neglected.

A most important characteristic of these profiles is that the shape of the profiles change very little with radius. The profile in one radial band is well approximated by that of a different radial band multiplied by a constant. In mathematical terms,

$$T'(r,z) \simeq \alpha(r)\hat{T}(z) \tag{19}$$

where $T'(r,z)$ is the temperature anomaly at height z and radius r, $\hat{T}(z)$ is an idealized temperature anomaly profile, and $\alpha(r)$ is a "strength" parameter. $\hat{T}(z)$ is slightly different in the two oceans. Although this result is based on the average storm, consistent findings have been reported for individual hurricanes by LaSeur and Hawkins (1963), Hawkins and Rubsam (1968), and Hawkins and Imbembo (1976).

The mean environments around Atlantic storms and West Pacific storms are very similar as shown in Figure 13 and Appendix I.

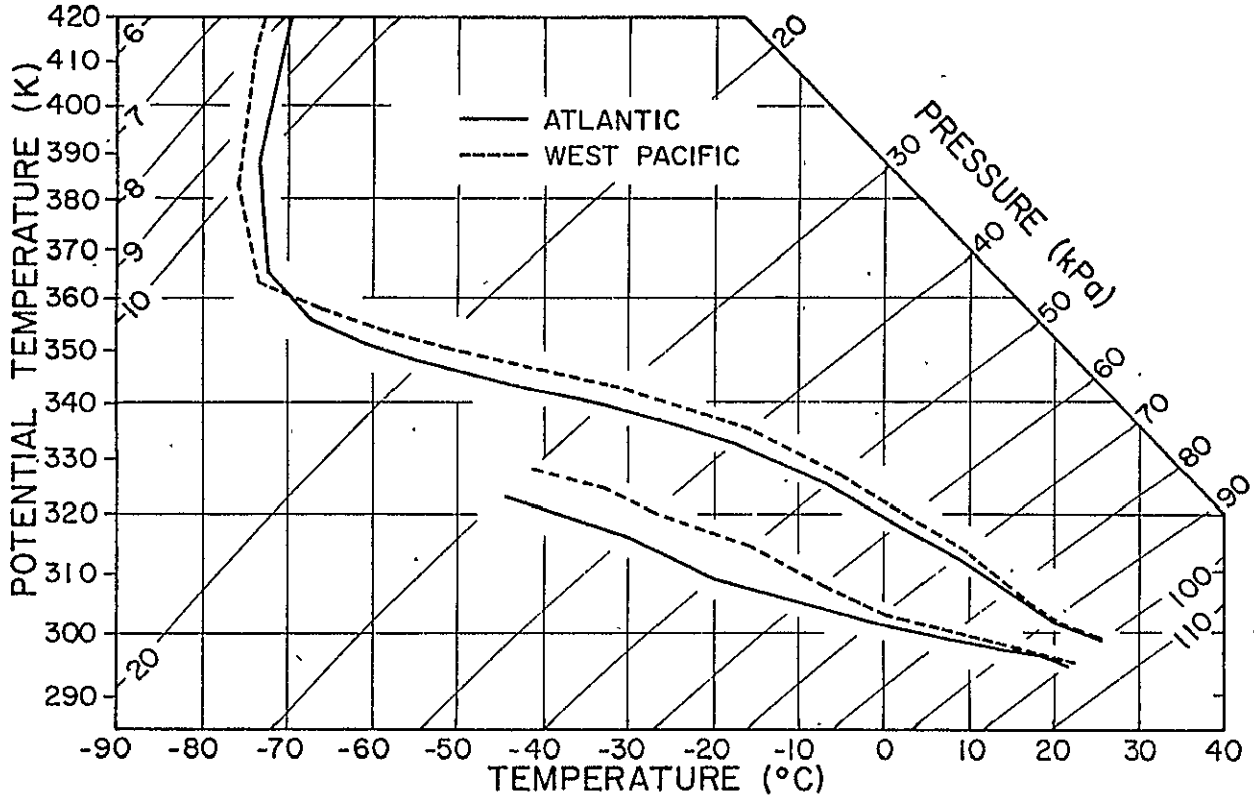

Figure 13. Mean environment of West Pacific typhoons and Atlantic (West Indies) hurricanes (after Núñez and Gray, 1977)

3.2 Satellite Observations

Because the warm temperature anomaly in a tropical cyclone is in the region sensed by the 55.45 GHz SCAMS channel, warm brightness temperature anomalies should be detectable in the data. Such anomalies were first observed over Typhoon June of 1975 by Rosenkranz and Staelin (1976) and were reported by Rosenkranz et al. (1978). In order to further investigate these anomalies, SCAMS data over eight typhoons and five hurricanes during 1975 (Table 4) were collected. It was found that warm 55.45 GHz brightness temperature anomalies exist over many storms. Figure 14 shows 55.45 GHz temperature anomalies over four storms of varying intensity. Figure 15 shows concurrent 11.5 μm THIR images of the storms. The temperatures plotted in Figure 14 are deviations from the environmental mean 55.45 GHz brightness temperature defined as the average brightness temperature between 4° and 10° from the storm center. Before any processing, all brightness temperatures were corrected for limb darkening (see next section) by adding a correction developed by Rosenkranz et al. (1978) and listed in Table 5. The warming in the center of June is striking; it reaches 4.1 K and extends several hundred kilometers from the storm center. Warming in less intense storms has a smaller magnitude and covers a smaller area. In Caroline, which was weak (25 m s^{-1}) at the time of the observation plotted in Figure 14, the warming is probably not detectable due to the $\pm$ 0.5 K noise level of the radiometer. As pointed out in Section 2.5, these warm brightness temperature anomalies are not caused by clouds or precipitation. Also, they are not caused by foam formation on the ocean surface because the transmittance from the surface to the satellite at 55.45 GHz is essentially zero (~ 10^{-4}). The anomalies represent real thermodynamic

Table 4

Storms used in this study (all 1975)

NAME	PEAK INTENSITY ($m\ s^{-1}$)	DATE/TIME OF PEAK INTENSITY	MINIMUM SEA LEVEL PRESSURE (kPa)	CENTRAL LOCATION AT TIME OF PEAK INTENSITY	
June	82	19 Nov/12Z	87.5	13.2N	141.0E
Phyllis	62	14 Aug/18Z	92.5	24.1N	137.1E
Rita	41	22 Aug/12Z	--	32.9N	134.4E
Tess	49	4 Sep/18Z	94.5	23.0N	147.6E
Winnie	33	10 Sep/06Z	--	31.0N	162.8E
Alice	39	17 Sep/12Z	97.3	15.4N	132.1E
Betty	49	22 Sep/00Z	94.7	22.6N	123.6E
Cora	54	4 Oct/18Z	94.3	30.3N	133.2E
Caroline	51	31 Aug/00Z	96.3	24.0N	97.0W
Doris	49	2 Sep/18Z	--	37.7N	44.2W
Eloise	57	23 Sep/06Z	96.1	28.4N	87.3W
Faye	43	26 Sep/18Z	97.9	31.0N	63.1W
Gladys	64	2 Oct/00Z	94.2	31.0N	73.0W

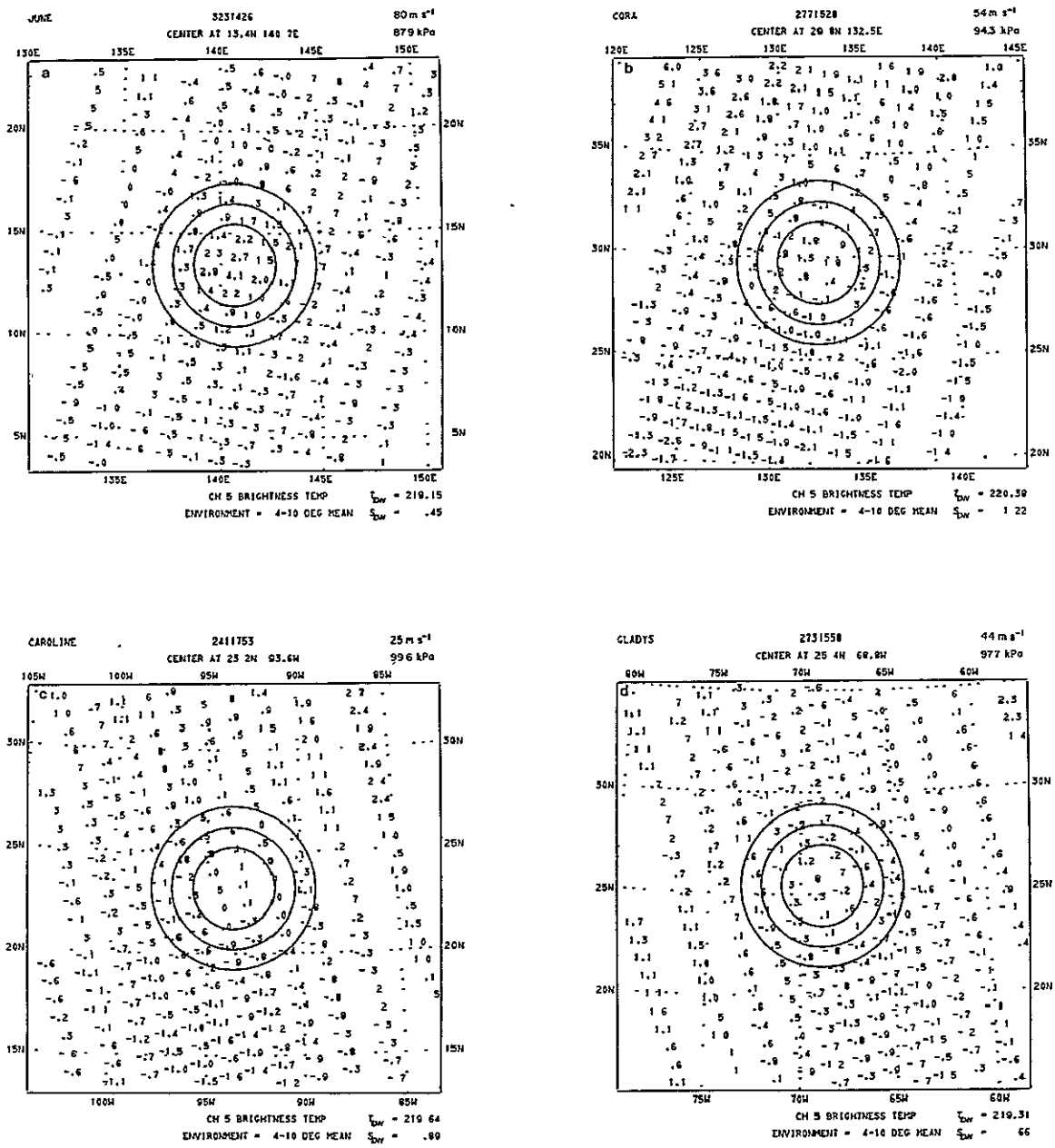

Figure 14. 55.45 GHz brightness temperature anomalies. The three circles are at radii of 2^{o}, 3^{o}, and 4^{o} from the interpolated best track storm center. The interpolated maximum wind speed and central pressure are shown in the upper right-hand corner. The environmental mean brightness temperature and its standard deviation are shown in the bottom right-hand corner. (a) Typhoon June on 19 November 1975 at 1426 GMT; (b) Typhoon Cora on 4 October 1975 at 1528 GMT; (c) Hurricane Caroline on 29 August 1975 at 1753 GMT; (d) Hurricane Gladys on 30 September 1975 at 1558 GMT

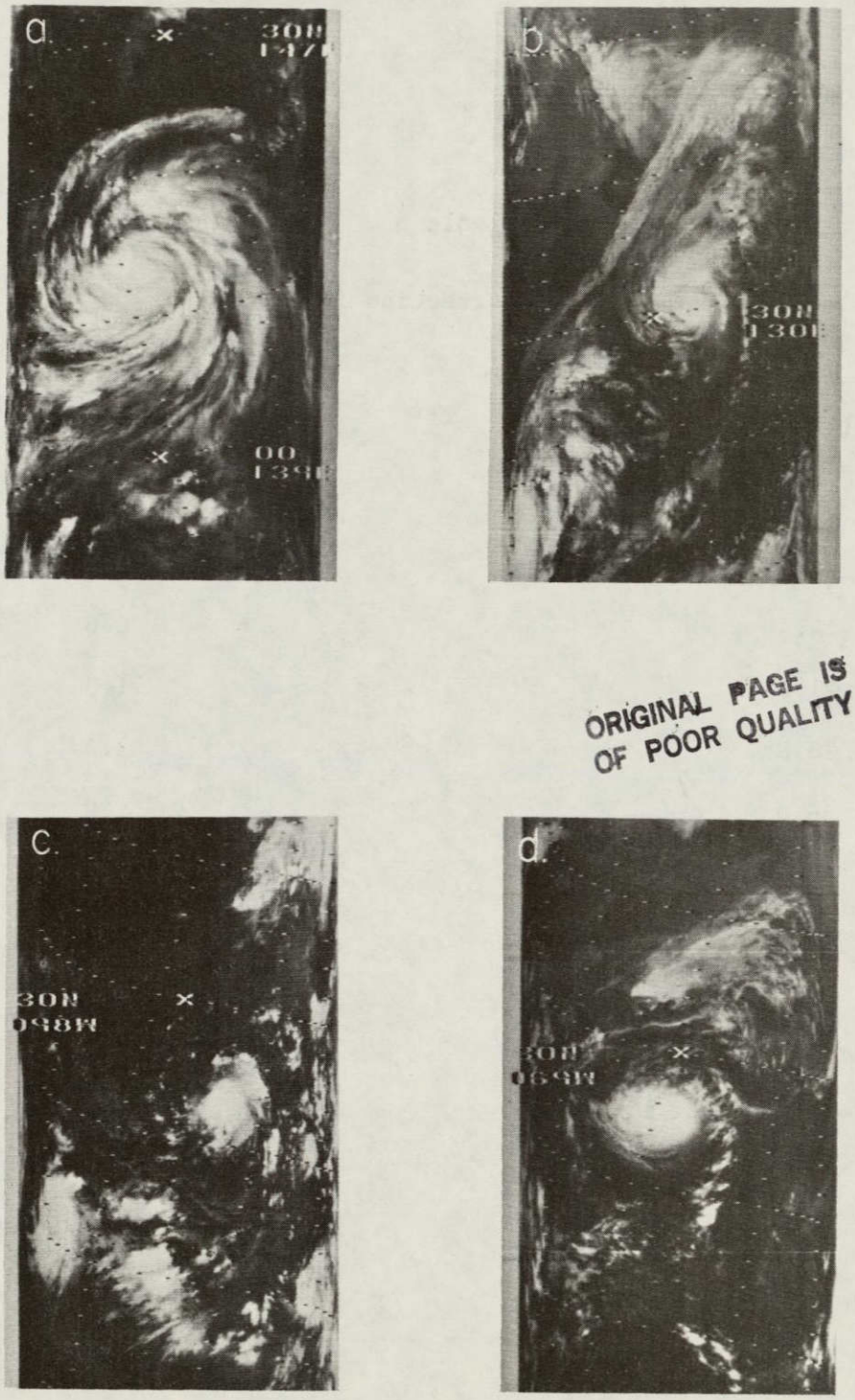

Figure 15. 11.5 μm THIR images of the four storms in Figure 14 (a) Typhoon June on 19 November 1975 at 1426 GMT: (b) Typhoon Cora on 4 October 1975 at 1528 GMT; (c) Hurricane Caroline on 29 August 1975 at 1753 GMT; (d) Hurricane Gladys on 30 September 1975 at 1558 GMT

Table 5

Limb Darkening Correction for 55.45 GHz

Scan Angle (deg)	Correction (K)
0	0.0
7.2	0.1
14.4	0.6
21.6	1.8
28.8	3.2
36.0	4.9
43.2	7.2

warming in the storms, a conclusion also reached by Rosenkranz et al. (1978). These results from the 13 storms were previously reported by Kidder et al. (1978).

3.3 Limb Darkening Correction

In Section 2.1 it was stated that although plane-parallel geometry is not strictly applicable to the present problem (temperature changes with radius in a tropical cyclone), it would be used because it does not affect the calculations done in this study. The reason for this is that the plane parallel assumption is necessary only for frequencies at which appreciable radiation from the surface is sensed by the satellite. The surface was modelled as a specular reflector with reflectance equal to $1 - \varepsilon(\theta)$. If the sky brightness temperature depends on azimuth angle (nonplane-parallel atmosphere), it is difficult to calculate the reflected contribution to the satellite observed brightness temperature. For frequencies which do not sense the surface, the plane-parallel geometry assumption may be dropped. For such frequencies, the ratio $\tau_{o,H}/\tau_{z,H}$ in Eq. (18) is one at the surface and decreases rapidly with height. The factor $d(\tau_{z,H}^{\sec\theta})/dz$ is significantly different from zero only far from the surface. Thus the weighting functions for frequencies which do not see the surface reduce to

$$W_\lambda(\theta,z) = \frac{d}{dz}\left(\tau_{z,H}^{\sec\theta}\right) , \tag{20}$$

and the brightness temperature measured by a satellite is

$$T_B(\theta) = \int_0^H W_\lambda(\theta,z)T(z)dz , \tag{21}$$

which is exactly the same formula one would have found by integrating the radiative transfer equation without the plane-parallel assumption. (T(z) is to be interpreted as the temperature encountered along the ray path at height z. It may be different for different paths).

At this point it is convenient to discuss the limb darkening correction mentioned in the last section and used throughout the rest of this study. As the scan angle of a satellite-borne microwave radiometer increases, its weighting function peaks at a higher level in the atmosphere (c.f. Figures 9-10). Since less of the warmer lower atmosphere is being viewed, the brightness temperature decreases. This process is known as limb darkening. Because it is inconvenient to try to compare brightness temperatures observed at different scan angles, a common practice is to develop a correction for limb darkening and then to treat all observations as if they were nadir observations. The limb darkening correction developed by Rosenkranz et al. (1978) and verified in this study for the 55.45 GHz SCAMS channel (Table 5) was computed by averaging observed brightness temperatures near the equator (where temperature gradients are small) as a function of scan angle. The mean brightness temperature at angle θ was found to be less than the mean nadir brightness temperature by an amount listed in Table 5. The correction consists simply of adding these temperatures to the observed brightness temperatures. That the corrections are so small, especially near nadir, indicates that the process will result in accurate brightness temperatures.

3.4 Surface Pressure Equation

Because the upper level warm temperature anomaly in a tropical cyclone is responsible for the surface pressure drop, measurements of

this warming can be used to estimate surface pressure anomalies or gradients (see Gray, 1977). The nadir brightness temperature* for a frequency which does not sense the surface is, from Eq. (21)

$$T_B = \int_0^H W_\lambda(z)T(z)dz \ . \tag{22}$$

Near a tropical cyclone we may divide $T(z)$ into environmental temperature, $T_E(z)$, and temperature anomaly, $T'(r,z)$, and use Eq. (19) to represent the anomaly:

$$T(r,z) = T_E(z) + \alpha(r)\ \hat{T}(z) \ . \tag{23}$$

Substituting into Eq. (22),

$$T_B(r) = T_{B_E} + \alpha(r) \int_0^H W_\lambda(z)\hat{T}(z)dz \ , \tag{24}$$

where T_{B_E} is the brightness temperature of the environment. The surface pressure can be calculated from the hydrostatic equation,**

$$\frac{d \ln p}{dz} = - \frac{g}{RT(z)} \tag{25}$$

Integrating in the vertical,

$$\ln\left[\frac{p_s(r)}{p_T}\right] = \frac{g}{R}\int_0^{H_T} \frac{dz}{T(z)} \tag{26}$$

where p_s is the surface pressure, and p_T and H_T are the pressure and height of some surface such as the 5 kPa surface which is undisturbed by the tropical cyclone below it (Frank, 1977). Using Eq. (23) and the

*Only nadir brightness temperatures need to be treated because the limb darkening correction will be applied to all observational data.

**See Appendix II for a demonstration that hydrostatic balance may be assumed in a tropical storm.

binomial expansion (keeping only the term linear in $\alpha(r)$),

$$\ln\left[\frac{p_s(r)}{p_T}\right] \approx \frac{g}{R}\int_0^{H_T}\frac{dz}{T_E(z)} - \frac{g}{R}\,\alpha(r)\int_0^{H_T}\frac{\hat{T}(z)}{T_E^2(z)}\,dz\ , \tag{27}$$

or

$$\ln p_s(r) = \ln p_E - \frac{g}{R}\,\alpha(r)\int_0^{H_T}\frac{\hat{T}(z)}{T_E^2(z)}\,dz\ . \tag{28}$$

Eliminating $\alpha(r)$ between Eqs. (24) and (28), we have

$$\frac{\Delta \ln p_s}{\Delta T_B} = -\frac{g}{R}\int_0^{H_T}\frac{\hat{T}(z)}{T_E^2(z)}\,dz\left[\int_0^{H} W_\lambda(z)\hat{T}(z)dz\right]^{-1} \equiv -A\ , \tag{29}$$

where Δ indicates a departure from the environmental value. If one uses any of the anomaly profiles in Appendix I and the 55.45 GHz weighting function shown in Figure 9, the value of A is about $1 \times 10^{-2}\ K^{-1}$. A is not very sensitive to environmental temperature which enters only through the $T_E^{-2}(z)$ and through $W_\lambda(z)$. Changing $T_E(z)$ from the 15° North Annual Atmosphere to the U.S. Standard Atmosphere, for example, only changes A by 12% in the Pacific. Nor is A very sensitive to $\hat{T}(z)$. Changing $\hat{T}(z)$ from a Pacific to an Atlantic curve changes A by about 11%.

A more accurate method for calculating A, which takes into account the small temperature variation of W_λ, is to calculate the brightness temperature and surface pressure for an environment than to recalculate both after perturbing the environment with a chosen $\hat{T}(z)$. Plotted in Figure 16 is the surface pressure (note slight logarithmic scale) versus 55.45 GHz brightness temperature which resulted when the mean Western Pacific environment was perturbed by the 2°-3° $\hat{T}(z)$

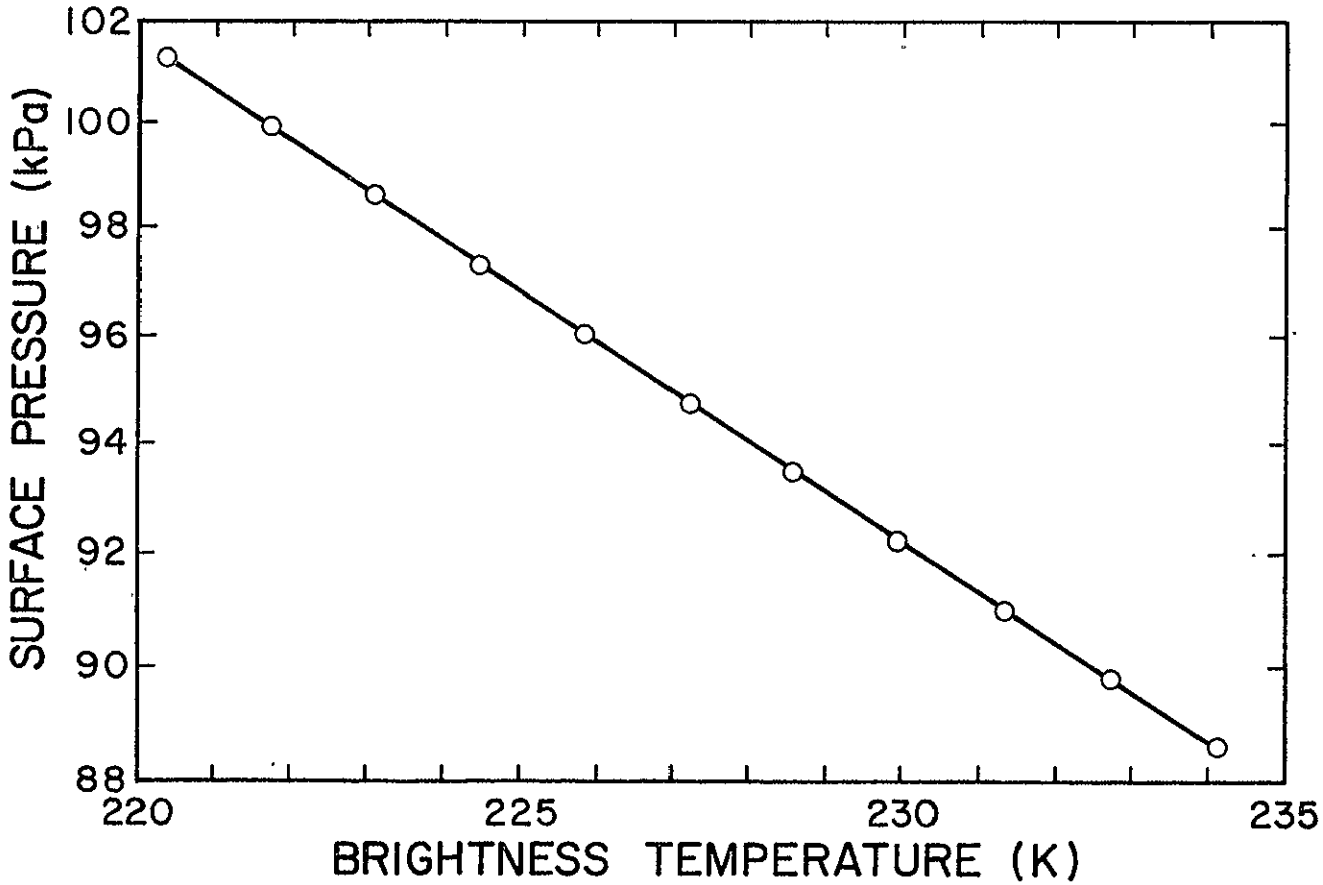

Figure 16. Surface pressure versus 55.45 GHz brightness temperature for α between zero and ten (Note: logarithmic surface pressure scale)

from the mean typhoon multiplied by a factor ranging from zero to ten. The linearity of the curve in Figure 16 indicates that the linear assumption used in deriving Eq. (29) is accurate. Table 6 lists the values of A calculated for the temperature anomaly profiles in Figure 12 and the appropriate environment. Values of A for both the Nimbus 6 SCAMS 55.45 GHz channel and the TIROS-N MSU 54.96 GHz channel are shown. The standard deviations listed are all less than 10% of the mean values, which gives an indication of the uncertainty in A.

Because the MSU 54.96 GHz channel has a weighting function which peaks closer to the level of maximum temperature anomaly in tropical cyclones (see Figures 9-10 and 12) it is potentially more useful than the 55.45 GHz SCAMS channel for the determination of surface pressure. Also, the 57.95 GHz MSU channel whose weighting function peaks at about 10 kPa could be useful for measuring cooling above the storm. The brightness temperatures from the 57.95 GHz and the 54.96 GHz channels could be used to estimate surface pressure in a two parameter equation of the form

$$\Delta \ln p_s = A\Delta T_{B_1} + B\Delta T_{B_2} , \qquad (30)$$

which should be more accurate than a single parameter fit.

All work in this study uses Eq. (29) in some form. It says simply that any gradient in the satellite-observed brightness temperature (at a frequency whose weighting function peaks in the upper troposphere) in a tropical cyclone is proportional to the gradient of the logarithm of the surface pressure. It means that for the first time surface pressure gradients or anomalies in tropical storms can be observed from satellites.

Table 6

Values of the Coefficient A (K^{-1})

	55.45 GHz	54.96 GHz
Atlantic		
0°-1°	1.13×10^{-2}	0.66×10^{-2}
1°-2°	1.10	0.66
2°-3°	1.07	0.64
3°-4°	1.03	0.62
4°-5°	1.01	0.62
5°-6°	0.94	0.54
6°-7°	0.85	0.51
Mean	1.02×10^{-2}	0.61×10^{-2}
Std. Dev.	0.09×10^{-2}	0.06×10^{-2}
Pacific		
0°-1°	0.90×10^{-2}	0.82×10^{-2}
1°-2°	0.94	0.83
2°-3°	0.98	0.84
3°-4°	0.99	0.86
4°-5°	1.02	0.87
5°-6°	0.95	0.85
6°-7°	0.83	0.80
Mean	0.95×10^{-2}	0.84×10^{-2}
Std. Dev.	0.06×10^{-2}	0.02×10^{-2}

3.5 Estimating Central Pressure from Satellite Data

One would like to be able to deduce the central pressure of a tropical cyclone from the satellite data. If one had a radiometer with high enough resolution to look down inside the eye, and if one knew the surface pressure of the environment, one could easily estimate the central pressure to within 1 kPa, assuming that the uncertainty in A is about 10%. A better knowledge of A would, of course, allow one to better estimate the central pressure. Accuracies to within 0.1 kPa may be possible.

The satellite data used in this study are all from the Nimbus 6 SCAMS which has a resolution of 145 km near nadir--much too coarse to accurately estimate central pressure. However, if the size of the eye does not vary too much, there should be a relationship between the brightness temperature of the eye and the central pressure, i.e. the logarithm of the central pressure should decrease linearly with brightness temperature:

$$\ln p_c - \ln p_E = -A(T_{B_{EYE}} - T_{B_E}) , \tag{31}$$

where p_c is the central surface pressure, p_E is the environmental surface pressure, $T_{B_{EYE}}$ is the eye brightness temperature, and T_{B_E} is the environmental brightness temperature. For the storms used in this study, we had no estimates of the environmental surface pressure. Fortunately, however, the surface pressure in the tropics varies only slightly in the absence of tropical cyclones; thus $\ln p_E$ can be considered a constant. Figure 17 shows a plot of $\ln p_c$ versus $\Delta T_B \equiv T_{B_{EYE}} - T_{B_E}$ for all typhoons* listed in Table 4 for which

*The two data points from hurricanes were excluded for consistency.

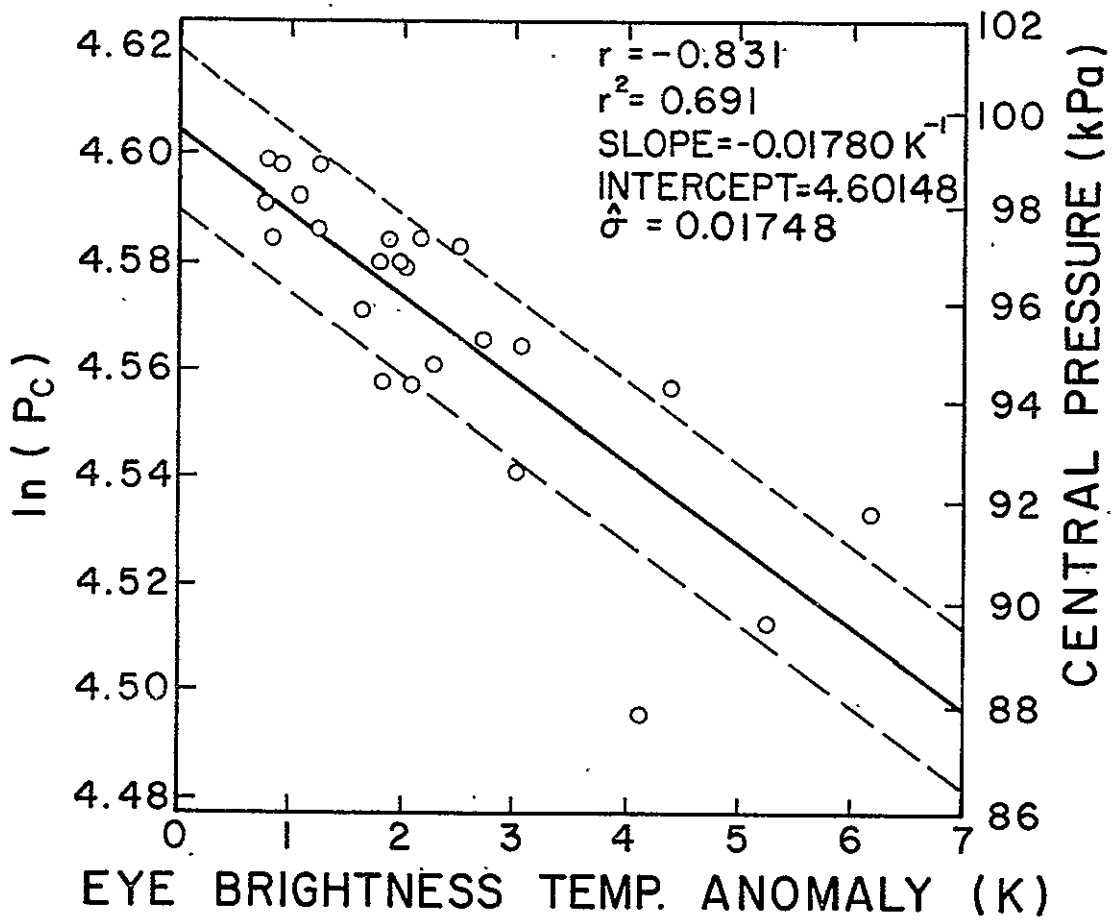

Figure 17. Logarithm of central pressure versus eye brightness temperature for eight typhoons during 1975

a) the eye brightness temperature was above the noise level of the radiometer ($\Delta T_B \geq 0.5$ K); b) the satellite viewing angle of the center of the storm was less than or equal to 28.8°; and c) a central pressure estimate was available.* The eye brightness temperature was determined as follows: The storm was positioned at the time of satellite observation by interpolating between 6 h best track locations. Then the maximum brightness temperature within 145 km (the distance between scan spots) of the interpolated center was labeled as the eye brightness temperature. The environmental brightness temperature was defined as the average of all brightness temperatures in a 5° latitude band centered on the eye which are at least 4° from the center of the storm; that is the average brightness temperature east and west of the storm was used as the environmental brightness temperature. All brightness temperatures were corrected for limb darkening.

Some of the possible causes of variance in Figure 17 are:

1) Radiometer noise.

2) Eye smaller than the radiometer resolution and of variable size.

3) Noncentering of the eye in the radiometer scan spot.

4) Variation of the shape of the temperature anomaly profile $\hat{T}(z)$ among the storms.

Particularly serious is the variability of the eye diameter. The three lowest pressure points in Figure 17 are all from Typhoon June. The left-most point (November 19, 1426 GMT) is near the time of peak intensity. The interpolated central pressure at this time was 87.9 kPa.

*Central pressure estimates, storm intensity and positions were obtained from the 1975 Annual Typhoon Report, Staff, JTWC (1976) and Hebert et al. (1977).

The two points to the right (November 20, 0213 GMT and November 21, 1445 GMT, respectively) represent the decaying stage. The central pressures were 89.6 kPa and 91.8 kPa, respectively. During this time period the eye brightness temperature was steadily increasing because the eye changed from a circle with a 5 n mi diameter to a 25 by 40 n mi ellipse (Staff, JTWC, 1976). This indicates that if one wants to accurately measure tropical cyclone central pressure with this method, either higher resolution radiometers or independent data on the size of the eye (probably both) are needed.

Figure 17 establishes that surface pressure falls as the 55.45 GHz brightness temperature rises (apart from problems with variable eye size). An interesting question, though, is why the slope of the regression line (1.78×10^{-2} K^{-1}) is not closer to the values of A listed in Table 6. There are two possible explanations. A likely explanation is that the variance caused by changes in the eye diameter has biased the statistics. A possible explanation is that the temperature anomaly profile $\hat{T}(z)$ for the eye of a tropical cyclone is qualitatively different than for the outer regions of the mean storm, on which data the calculation of A was based. At this point it can only be said that this technique for measuring the central pressure of tropical cyclones appears promising, but more research and higher resolution instruments are needed.

With the knowledge of how to relate brightness temperature gradients to surface pressure gradients, it is possible to estimate surface wind speeds. The SWIM technique is developed in the next chapter.

4.0 DETERMINATION OF THE OUTER WIND FIELD

If there is a more important measure of tropical cyclone strength than central pressure, it is surface wind speed. In this chapter the Surface Wind Inference from Microwave data (SWIM) technique will be developed by applying the results of the last chapter.

4.1 Theory

Because very little is known about the detailed variation of wind speed with height in the boundary layer of tropical cyclones (Bates, 1977), a simple approach will be taken. The wind speed at approximately the 85 kPa level, which Frank (1977) found to be the level of maximum wind speed in the mean typhoon, will be calculated and multiplied by a shearing parameter μ to estimate the surface wind speed. Bates (1977) suggests that μ is near 0.7. The effects of this choice will be discussed later.

The wind at the 85 kPa will be assumed to be in gradient balance, and a symmetric vortex will be assumed; thus

$$\frac{V_G^2}{r} + f\, V_G = RT_G \frac{\partial \ln p}{\partial r}\,, \tag{32}$$

where T_G is the temperature near 85 kPa, and f is the Coriolis parameter. Because the radial temperature gradient is nearly zero below 85 kPa, the following approximation may be made:

$$\frac{\partial}{\partial z}\left(\frac{\partial \ln p}{\partial r}\right) = \frac{\partial}{\partial r}\left(\frac{\partial \ln p}{\partial z}\right) = \frac{\partial}{\partial r}\left(-\frac{g}{RT}\right) \simeq 0\,. \tag{33}$$

Thus, the surface value of $\partial \ln p/\partial r$ may be used to approximate the value at gradient wind level (85 kPa). Substituting from Eq. (29) gives

$$\frac{V_G^2}{r} + f V_G = - ART_G \frac{\partial T_B}{\partial r} \tag{34}$$

If one had high resolution, low noise satellite data, one could calculate the radial brightness temperature gradient and obtain the wind speed near 85 kPa directly from Eq. (34). However, because current satellite data is rather noisy ($\pm$ 0.5 K) and because it has rather coarse spatial resolution (145 km at nadir), direct calculations of wind speeds can be very noisy. A more useful approach is to assume that the wind speed, as a function of radius, takes a certain form. This has the effect of smoothing the wind speed estimates. A suitably simple function, suggested by Hughes (1952) and Riehl (1954, 1963) is

$$V = Cr^{-x} . \tag{35}$$

In the outflow region (15-25 kPa) x is approximately one; that is, parcels are attempting to conserve their angular momentum (ρrv). At low levels friction becomes important. Gray and Shea (1973) and Riehl (1963) have shown that 0.5 is the best value of x in the inner core ($r \leq 100$ km and $r >$ radius of maximum winds). It is possible that for r greater than 100 km, a value of 0.7 may be more appropriate for x. This point will be discussed later.

Substituting Eq. (35) into Eq. (34) gives

$$\frac{\partial T_B}{\partial r} = - (ART_G)^{-1} \left[C^2 r^{-2x-1} + f\, Cr^{-x} \right] \tag{36}$$

Holding A, C, x, f, and T_G constant and integrating with respect to r yields

$$T_B - T_C = (ART_G)^{-1} \left[C^2 \frac{r^{-2x}}{2x} - fC \frac{r^{1-x}}{1-x} \right] , \tag{37}$$

where T_C is an integration constant. If one has a field of satellite-observed brightness temperatures over a tropical cyclone, one can find the value of C in Eq. (37) which gives the best fit to the brightness temperatures for a given x. The value of C which gives the least squares best fit to the brightness temperature field is the positive real root* of the following equation:

$$\begin{aligned} &\frac{1}{x^2}\left[\sum r^{-4x} - \frac{1}{N}\left(\sum r^{-2x}\right)^2\right] C^3 \\ &\quad - \frac{3f}{x(1-x)}\left[\sum r^{1-3x} - \frac{1}{N}\left(\sum r^{-2x}\right)\left(\sum r^{1-x}\right)\right] C^2 \\ &\quad + \left\{\frac{2f^2}{(1-x)^2}\left[\sum r^{2-2x} - \frac{1}{N}\left(\sum r^{1-x}\right)^2\right]\right. \\ &\quad \left. - \frac{2}{x}\left[\sum yr^{-2x} - \frac{1}{N}\left(\sum y\right)\left(\sum r^{-2x}\right)\right]\right\} C \\ &\quad + \frac{2f}{1-x}\left[\sum yr^{1-x} - \frac{1}{N}\left(\sum y\right)\left(\sum r^{1-x}\right)\right] = 0 , \end{aligned} \tag{38}$$

where $y = ART_GT_B$. To eliminate the problem of an increasing number of points at distances further from the storm center, the brightness temperatures were averaged in 0.5° (56 km) radial bands before inserting

*It is observed that Eq. (38) has only one real positive root. The other two are generally real and negative, although they are sometimes complex conjugates. Occasionally, for weak storms, no positive real root is found.

in Eq. (38). With a knowledge of C, one may estimate surface wind speed from

$$V_o = \mu C r^{-x} . \tag{39}$$

In summary, the SWIM technique for estimating surface wind speeds around tropical cyclones from satellite-observed brightness temperatures is as follows:

1) Average the brightness temperatures in 56 km (0.5°) radial bands around the storm center.

2) Choose an appropriate value of x (see below).

3) Calculate C using Eq. (38) with A from Table 6.

4) Choose a value for μ (see below).

5) Estimate the surface wind speed for radii greater than the radius of maximum wind with Eq. (39).

6) Take into account asymmetries caused by storm motion by adding the storm motion to calculated wind speeds in the right quadrant and subtracting the motion in the left quadrant (see George, 1976).

It remains to determine the values of x and μ. Two types of data were used for this purpose: Nimbus 6 SCAMS 55.45 GHz data and simulated satellite data constructed from multilevel aircraft reconnaisance flights.

4.2 Aircraft Data

The first test of the above theory utilized aircraft reconnaissance data collected by the National Hurricane Research Project. Aircraft data were chosen because from it simulated satellite data could be constructed with very fine spacial resolution (4.6 km or 2.5 n mi), and accurate low level wind observations at the same resolution are available for comparison. To be useful in this study the aircraft had

to penetrate the storm at three or more levels: one at low levels to measure low level winds, one near 30 kPa to measure the upper level temperature anomaly, and one between the other two levels to specify middle level temperatures. Between 1957 and 1969 there were five days (four storms) during which such data were taken. All of the data used in this simulation (summarized in Table 7) were smoothed vortex averages from Gray and Shea (1976).

To construct the simulated satellite data, soundings were first constructed at each radial grid point using temperature and pressure data at each flight level and heights at the lowest flight level. Relative humidities were obtained from the mean storm environment (Appendix I). Between flight levels, the equivalent potential temperature was assumed to vary linearly with pressure (LaSeur and Hawkins, 1963). Above the upper-most flight level, the mean environmental sounding (Appendix I) was used, starting at 12.5 kPa. Finally, the 55.45 GHz brightness temperature was calculated from the constructed sounding.

For radii outside the radius of maximum wind speed, the calculated brightness temperatures were inserted into Eq. (38) to calculate C for x = 0.5, A = 1.02 x 10^{-2} K^{-1}, and T_G = 17.2°C. The offset T_C was also calculated and the brightness temperatures plus the best fit curve from Eq. (37) are shown in Figure 18. It can be seen, particularly in the case of Inez, that Eq. (38) gives a good fit to the calculated brightness temperatures. The calculated wind speed at the gradient (~ 85 kPa) level ($V_G = Cr^{-x}$) and the smoothed, vortex averaged, observed total wind speed at the lowest flight level are plotted in Figure 19 in which both scales are logarithmic. Except for

Table 7

Summary of Aircraft Reconnaissance Data from Hurricanes Used in this Study

Storm	Date	Flight Levels (kPa)	Intensity Change
Cleo	18 Aug 1958	80,56,24	Steady
Helene	26 Sep 1958	80,56,25	Deepening
Hilda	1 Oct 1964	90,75,65,50,18	Deepening
Hilda	2 Oct 1964	90,70,65,20	Filling
Inez	28 Sep 1966	95,75,65,50,20	Deepening

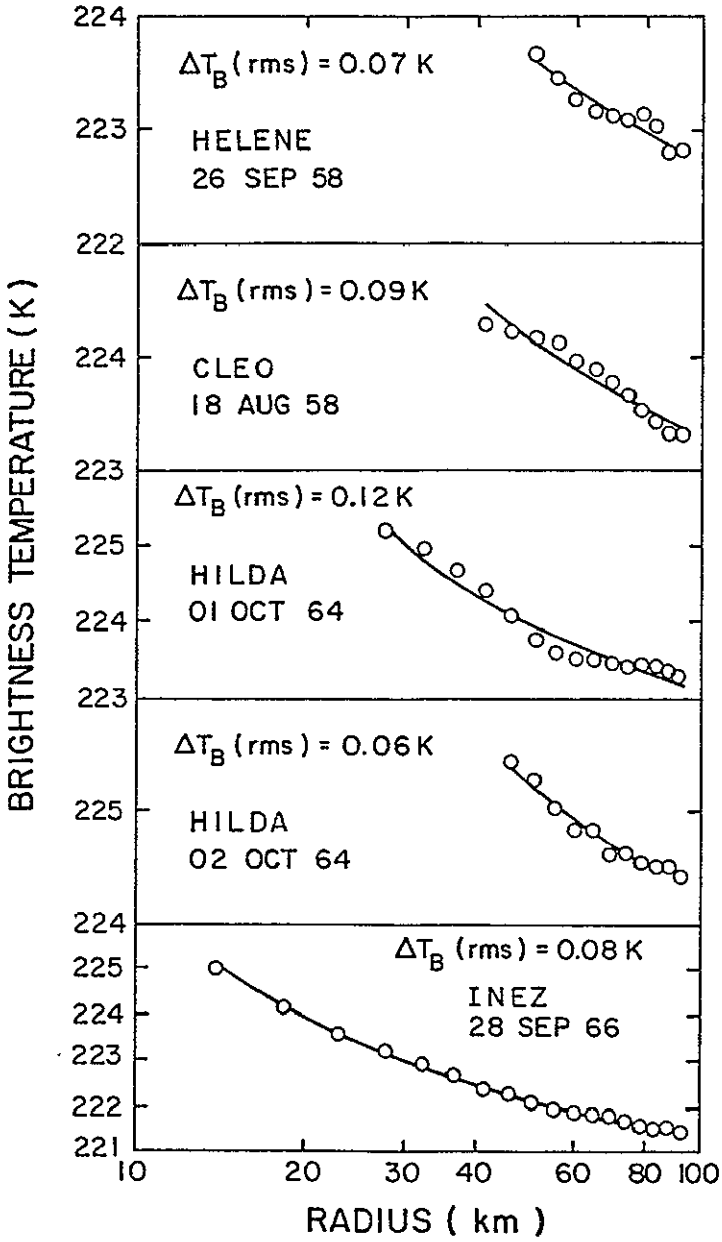

Figure 18. Calculated 55.45 GHz brightness temperatures (circles) and best fit line for four hurricanes

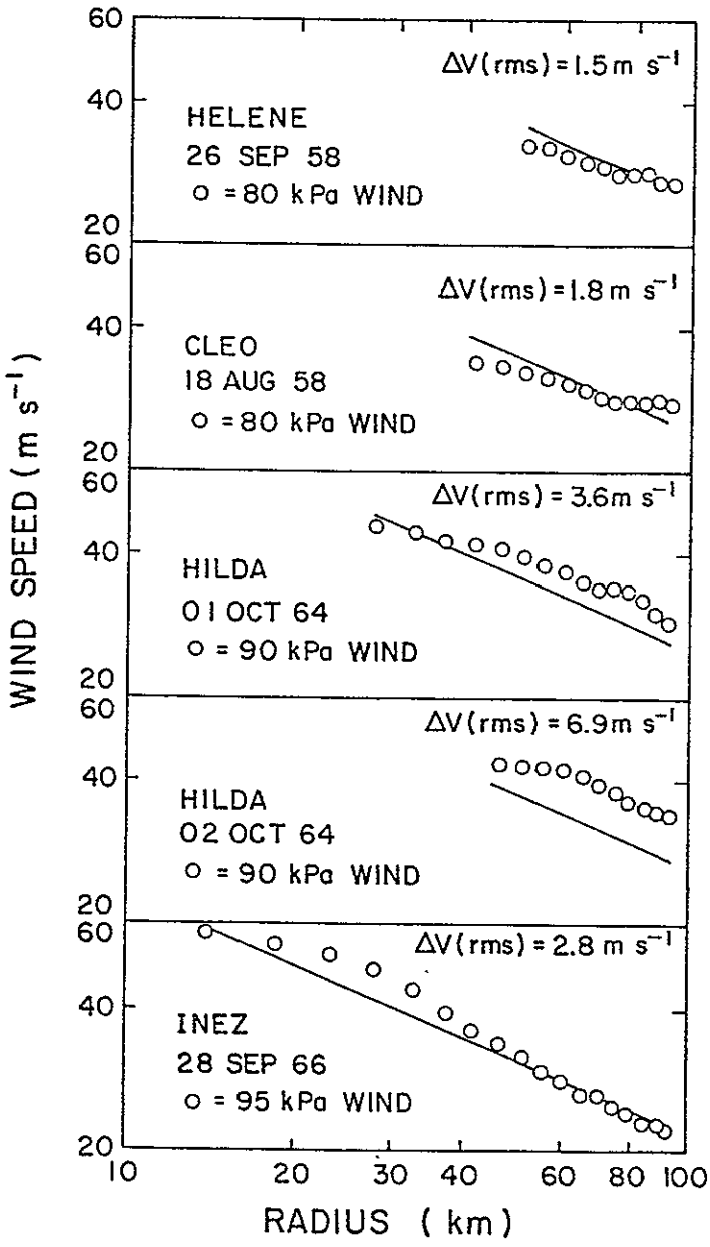

Figure 19. Calculated gradient level (~ 85 kPa) wind speeds (line) and observed low level wind speeds for four hurricanes (note that both scales are logarithmic)

Hilda on October 2, 1964, the agreement between the observed and calculated wind speeds is excellent with rms errors of 2-3 m s^{-1}. This uncertainty is very small considering that the observed winds and the calculated winds are not for the same level.

The case of Hilda on October 2 is interesting because it is the only filling storm. It is possible that storm temperature structure is different enough in later stages that A should have a different value. It is also possible that the process of constructing soundings mentioned above failed to detect the true intensity of Hilda in terms of upper level temperature anomaly. This may have caused the calculated brightness temperature gradient (and thus the calculated winds) to be too low. More research is needed to adequately answer this question, and a program to obtain the answer will be discussed in the next chapter.

In summary it appears that with 4-5 km resolution satellite data, one could deduce low level tropical cyclone wind speeds. In the next section, data from the Nimbus 6 SCAMS, which has lower resolution, will be used to estimate surface wind speeds in eight typhoons during 1975.

4.3 Nimbus 6 Data

From the tropical cyclones listed in Table 4 data consisting of 116 Nimbus 6 SCAMS, 55.45 GHz brightness temperature images were screened to meet the following criteria: a) the scan angle to the storm center was less than or equal to 21.6°, and b) an independent estimate of the radius of 15.4 m s^{-1} (30 kt) wind was available. Only 20 images met both criteria, and only one of these was in the Atlantic; the remainder were Pacific typhoons. To make the data set uniform, Tropical Storm Gladys (the only Atlantic storm) was eliminated, leaving 19 images of

eight typhoons. This is a rather small data set, but it is large enough to indicate the potential of the SWIM technique.

Using the maximum brightness temperature within 145 km (distance between scan spots at nadir) of the interpolated best track center (1975 Annual Typhoon Report) as in Chapter 3, the 55.45 GHz SCAMS brightness temperatures were averaged in 56 km (0.5°) radial bands from 111 km (1°) to 778 km (7°). The eye brightness temperature was not included in the fitting process. In the first analysis, the azimuthally-averaged brightness temperatures were used in Eq. (38) to calculate C for x = 0.5, A = 0.95×10^{-2} K^{-1}, and T_G = 17.2°C. The radii of 15.4 m s^{-1} (30 kt) and 25.7 m s^{-1} (50 kt) winds were calculated using μ = 0.7 to estimate surface wind speeds. These calculations are compared with observations in Figure 20.

The "observed" radii were obtained as follows: each six hours the forecaster on duty at the Joint Typhoon Warning Center estimates the radii of 30 kt, 50 kt and 100 kt winds from all data sources.* The observed value used in this study is the average radius both around the storm and from the time periods just before and just after the satellite image. Being subjective estimates based on all available data sources, it is reasonable to assume that the observed radii are overestimated. Since safety is the prime consideration, it is better to overestimate than to underestimate. The average value of this error is unavailable.

*These estimates were supplied to the author by LCDR David Sokol of the Joint Typhoon Warning Center, Guam, and by Mr. Samson Brand of the Naval Environmental Prediction Research Facility, Monterey, Calif.

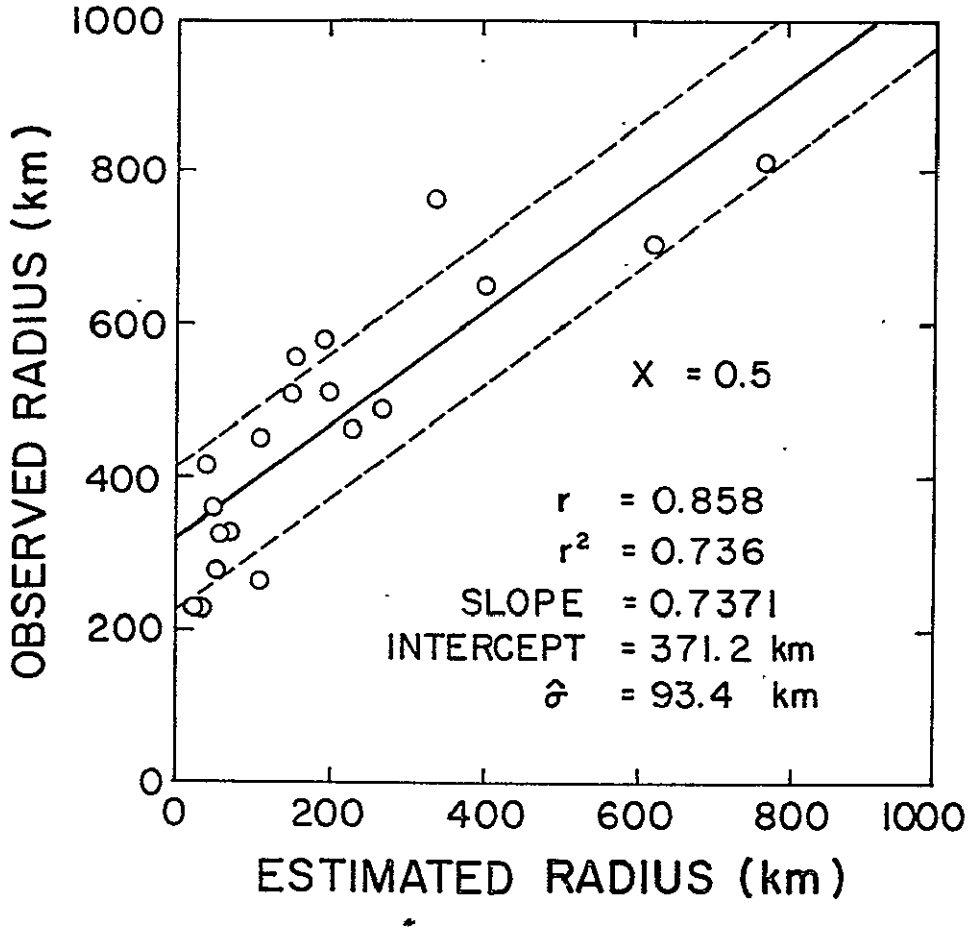

Figure 20a. Observed versus estimated average radius of 15.4 m s^{-1} (30 kt) winds in eight typhoons during 1975 for x=0.5

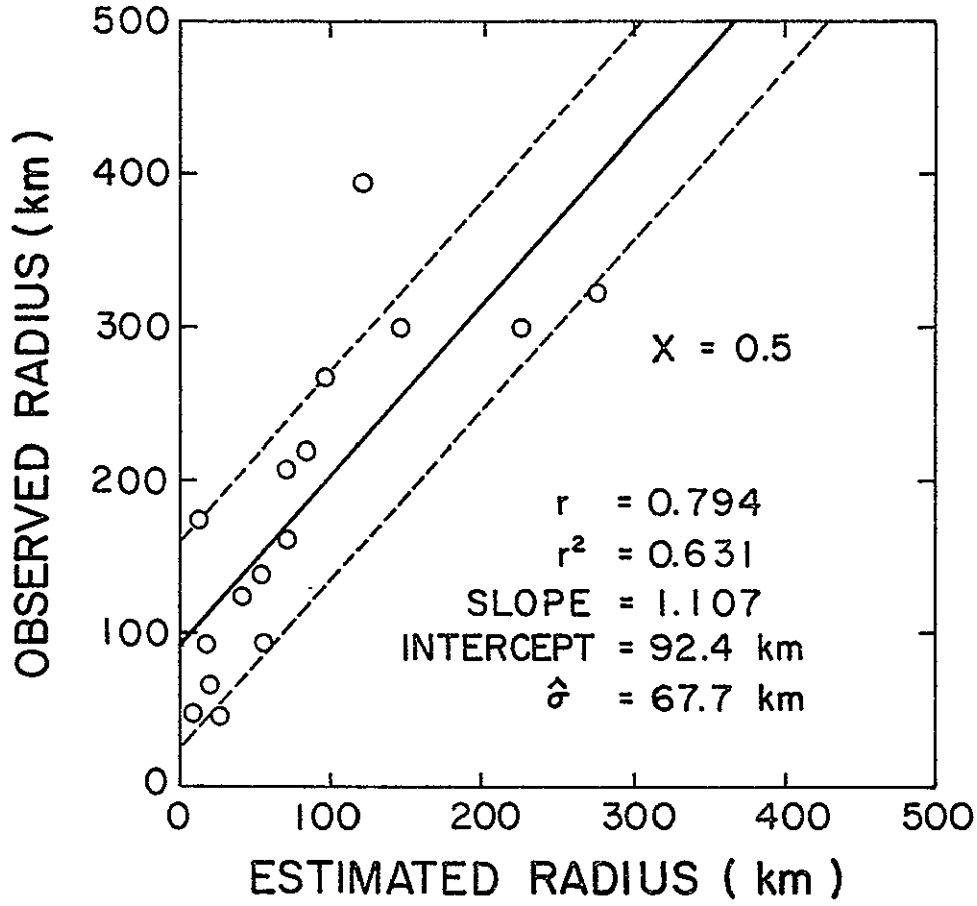

Figure 20b. Observed versus estimated average radius of 25.7 m s^{-1} (50 kt) winds in eight typhoons during 1975 for x=0.5

Because the data set is so small, the data were not screened for quality. Still, the regression lines in Figure 20 explain 63% to 74% of the variance for 25.7 m s^{-1} (50 kt) and 15.4 m s^{-1} (30 kt) winds, respectively. The standard errors of estimate are 68 km and 93 km, respectively, which are reasonably good, and which may be influenced by the nature of the "observed" values. The intercepts are rather large, but some of this error is accounted for by the natural overestimation in the observed radii discussed above.

If the theory is correct, the slopes should be near one. The fact that the slope for the radius of 15.4 m s^{-1} wind is somewhat less than one leads one to speculate about the best values of the shearing parameter μ and the wind exponent x to use in the analysis. Bates (1977) suggests that μ is about 0.7, but a variation from 0.6 to 0.8 is not unrealistic. For r less than 100 km, 0.5 is a good value for x, but Malkus and Riehl (1959) suggest that between 200 km and 500 km, x should be 0.6 to 0.7. Even though very few data points are available an analysis was undertaken to determine the effects of different μ's and x's. It should be first noted that the regression coefficient, the intercept, and the standard error of estimate are unaffected by the choice of μ. From Eq. (39) it can be seen that the radius of a particular value of surface wind speed is given by

$$r = \mu^{1/x}\left(\frac{C}{V}\right)^{1/x} \tag{40}$$

Changing μ has the effect of rescaling the abscissa, which will only change the slope of the regression line.

Table 8 shows the square of the regression coefficient, the standard error of estimate, the slope and the intercept of the least

Table 8

Variation of regression statistics as functions of x and μ

x	r^2	Intercept (km)	σ (km)	Slope μ=0.6	Slope μ=0.7	Slope μ=0.8
			Radius of 15.4 m s^{-1} (30 kt) Wind			
0.4	0.680	349	103	0.810	0.551	0.395
0.5	0.736	317	93	1.003	0.737	0.564
0.6	0.771	285	86	1.183	0.915	0.732
0.7	0.801	251	81	1.359	1.090	0.901
0.8	0.820	217	77	1.534	1.265	1.071
			Radius of 25.7 m s^{-1} (50 kt) Wind			
0.4	0.579	111	72	1.555	1.058	0.758
0.5	0.631	92	68	1.507	1.107	0.848
0.6	0.663	74	65	1.506	1.165	0.933
0.7	0.685	55	63	1.534	1.231	1.017
0.8	0.701	36	61	1.582	1.305	1.104

squares best fit regression lines as functions of x and μ. In general, increasing x slightly increases the fraction of explained variance, increases the slope (except for μ=0.6), decreases the intercept, and slightly decreases the standard error of estimate. Increasing μ decreases the slope. For 25.7 m s^{-1} winds, it appears that μ=0.6 is too small; a slope of one is not produced for any x. For μ in the 0.7 to 0.8 range, an x of 0.4 to 0.7 produces the desired slope of one. Because the radius of 25.7 m s^{-1} winds is often fairly close to 100 km where x has been shown to be 0.5, the best value of x for 25.7 m s^{-1} winds is probably 0.5. With x=0.5, a μ in the range of 0.7 to 0.8 produces a regression line slope of about one.

For the radius of 15.4 m s^{-1} winds, a somewhat larger x seems appropriate. As μ varies from 0.6 to 0.8, the value of x needed to produce a slope of one varies from 0.5 to 0.8. Although μ may vary as a function of radius, there is no evidence that it does so. Using μ=0.7 as suggested by Bates (1977), the best value of x for 15.4 m s^{-1} winds is 0.7. The associated value of the intercept is 251 km, which is still rather large, and of the standard error of estimate is 81 km. Figure 21 shows the effect of changing x to 0.7 (μ=0.7). It seems to be a better fit for 15.4 m s^{-1} winds, but not as good for 25.7 m s^{-1} winds.

It should be noted that no useful information on the value of x was obtained when the error in fitting the azimuthally-averaged brightness temperatures was investigated. The rms error is about 0.1 K regardless of the value of x.

In summary, we have shown that with 145 km 55.45 GHz SCAMS data, one can estimate the radius of 15.4 m s^{-1} winds to within about

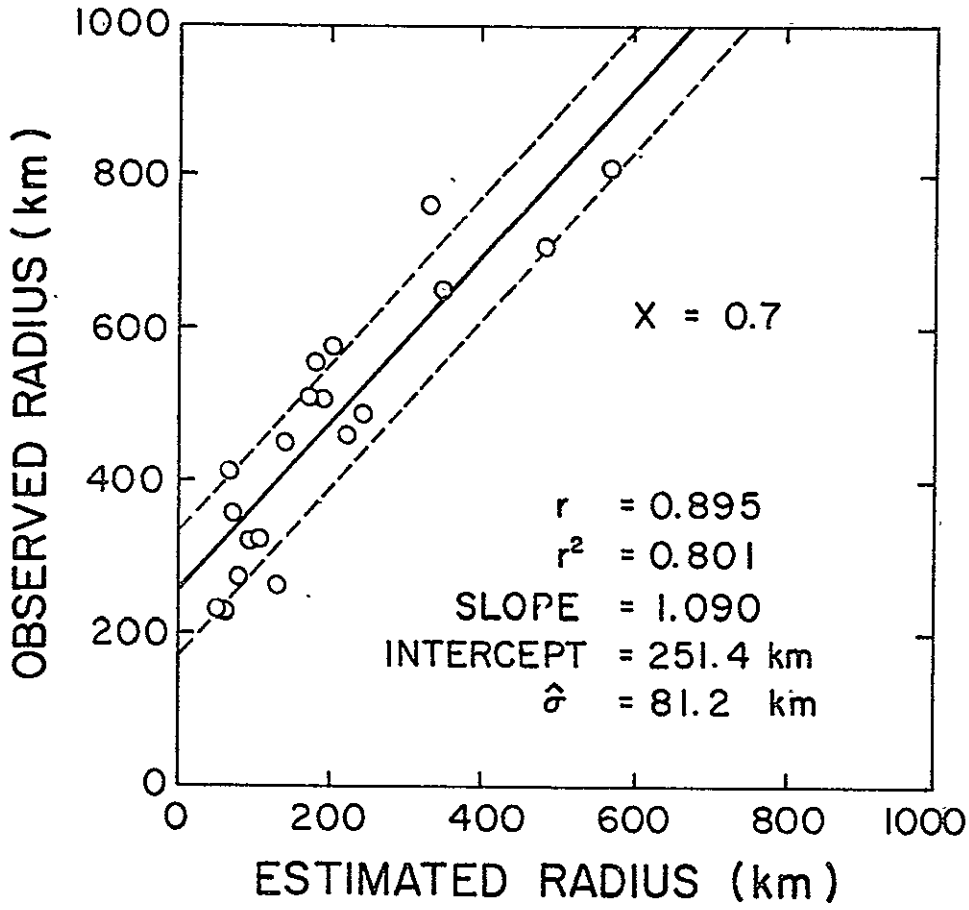

Figure 21a. Observed versus estimated average radius of 15.4 m s^{-1} (30 kt) winds in eight typhoons during 1975 for x=0.7

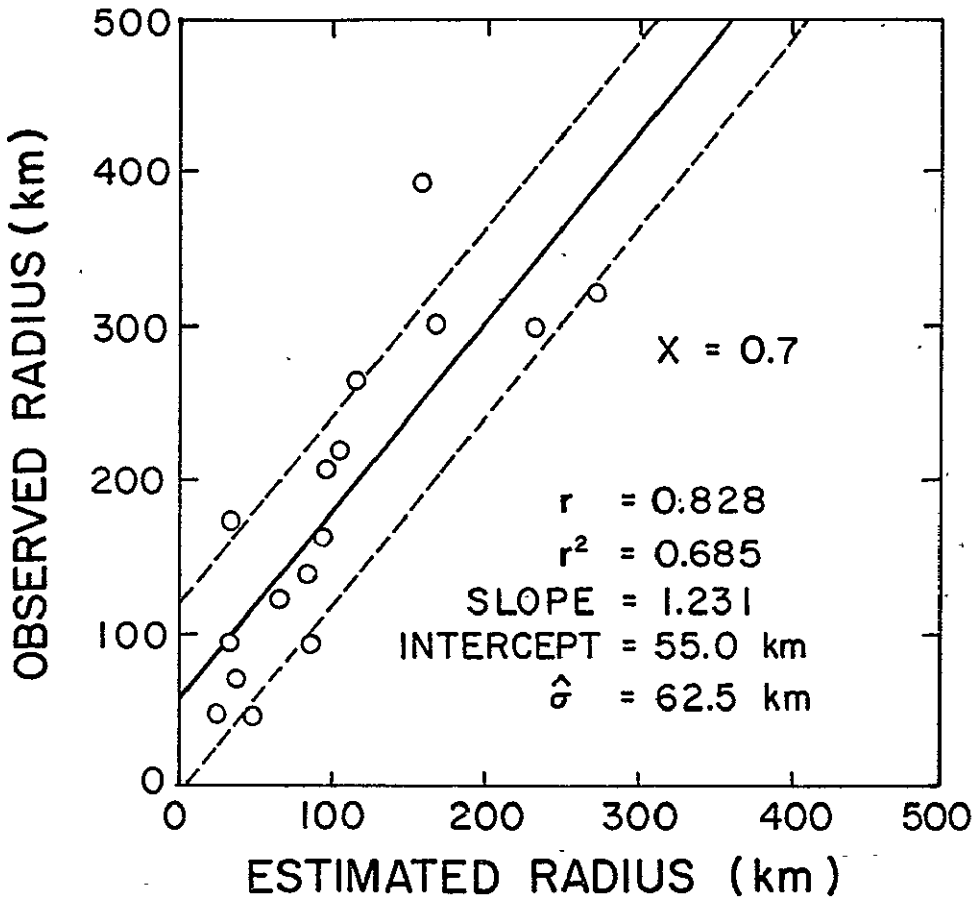

Figure 21b. Observed versus estimated average radius of 25.7 m s^{-1} (50 kt) winds in eight typhoons during 1975 for x=0.7

80 km (x=0.7) and the radius of 25.7 m s^{-1} winds to within about 65 km (x=0.5) using the SWIM technique. These values may improve if satellite estimates are compared with more exact observations. Of course the SWIM technique produces only azimuthally-averaged winds. In practice, asymmetries in the wind field produced by the motion of the storm (average speed ~ 5 m s^{-1}) need to be taken into account by adding the storm speed to the calculated wind speed in the right quadrant and subtracting the motion in the left quadrant (George, 1976).

On the basis of the results presented here, it appears that the SWIM technique has the potential to accurately estimate surface wind speed around tropical cyclones. Before the technique is ready for operational use, however, more research is needed. The next chapter outlines several steps which should be taken to improve and better assess the accuracy of the SWIM technique.

5.0 SUGGESTED FUTURE WORK

In Eq. (37) it can be seen that for a given tropical cyclone (given x and C), the signal above background is inversely proportional to A. Because A for the 54.96 GHz TIROS-N MSU channel is smaller than that for the 55.45 GHz SCAMS channel, MSU data should give about a 67% greater signal in the Atlantic and a 13% greater signal in the Pacific than SCAMS. The MSU also has a little better resolution than SCAMS (110 km versus 145 km) and a smaller noise equivalent temperature (0.3 K versus 0.5 K). Also, the 57.95 GHz MSU channel may be coupled with the 54.96 GHz channel to give a two parameter estimation of the surface pressure gradient (see Section 3.4). For all of the above reasons, the SWIM technique should be tested on TIROS-N MSU data.

Another useful experiment would be an aircraft reconnaissance experiment. If a microwave sounder were mounted on an aircraft such as a U-2 (cruising altitude approximately 20 km) which can fly over the top of tropical cyclones, one could simulate very high spatial resolution satellite data. If there were simultaneous flights by more conventional aircraft (e.g. NOAA P-3's from Miami, or NASA's Convair 990) at the level of maximum temperature anomaly (25-30 kPa) and at low levels to measure wind speeds, very detailed information on storm structure could be obtained, and the SWIM technique could be thoroughly tested. New techniques could also be developed from such data. Data from channels with weighting functions which peak in the lower atmosphere could be combined with upper level weighting functions to produce vertical temperature profiles within the storms which may be useful in forecasting motion or intensity changes. With high spacial resolution, it should

be possible to estimate storm central pressure as outlined in Chapter 3. Also, it might be possible to infer wind speeds inside the eye of the storm. It has been suggested that inside of the eye, the wind speed is approximately proportional to the radius. With an estimate of surface pressure gradient inside of the eye, it might be possible to estimate wind speeds. If so, knowledge of wind speeds inside and outside of the eye might be combined to estimate maximum wind speed. Such information would be extremely useful both to modellers and to forecasters.

Finally, and further in the future, Spacelab will provide an ideal platform for testing the feasibility of designing a satellite instrument specifically for observations of tropical cyclones. Orbital inclinations from 28.5° to 104° and altitudes from 200 km to 900 km (Spacelab User's Guide) insure good coverage of tropical regions. High spatial resolution, accurately earth located data should be obtainable. The Instrument Pointing Subsystem (IPS) has been designed to be capable of pointing a 3 m dish antenna with a one second accuracy. Such a platform will allow detailed observations of tropical cyclones.

6.0 SUMMARY AND CONCLUSIONS

A new approach to the problem of estimating surface wind speed and pressure around tropical cyclones has been presented. The Surface Wind Inference from Microwave data (SWIM) technique uses satellite microwave sounder data to measure the upper tropospheric temperature anomalies which are responsible for the central pressure drop and thus the high winds. Because the microwave data are not significantly affected by clouds and precipitation, the technique can be used regardless of cloud cover. The satellite measured brightness temperatures were related through the radiative transfer and hydrostatic equations to the surface pressure. Although current satellite instruments have too coarse a resolution to accurately measure central pressure, future instruments may be able to do so with 0.1 kPa accuracy. Surface pressure gradients were then related to surface wind speed through the gradient wind equation and a shearing parameter. The SWIM technique was tested first using simulated satellite data constructed from aircraft reconnaissance flights. With this high resolution (4.6 km) simulated data, 80-95 kPa wind speeds were estimated with accuracies of 2-3 m s^{-1}. Second, the SWIM technique was tested using 55.45 GHz brightness temperature data from the Nimbus 6 SCAMS over eight typhoons during 1975. The technique was used to estimate the radii of 15.4 m s^{-1} (30 kt) and 25.7 m s^{-1} (50 kt) winds. Although very few data points were available for analysis, it appears that the radius of 15.4 m s^{-1} winds were determined to within about 80 km and the radius of 25.7 m s^{-1} winds to within 65 km. Data from the TIROS-N MSU 54.96 GHz channel, because it produces a larger signal above background, should produce better results.

In conclusion, the SWIM technique for estimating surface pressures and wind speeds appears very promising and deserves further research. It is a simple method based on the radiative transfer, hydrostatic, and gradient wind equations. It is an objective technique which requires little computing time. In short, it is a strong candidate for an operational tool.

If we are to be able to better forecast tropical cyclone motion and intensity change we must have much better knowledge of the dynamic and thermodynamic structure of individual storms and of their environments. The author believes, for example, that many mesoscale numerical models, including tropical cyclone models, are much better than the data with which they are initialized. The only way to obtain the mesoscale data necessary to initialize the models is to mount sensors on satellite platforms. However, data from satellites is not sufficient. Techniques such as the SWIM technique must be developed which translate the satellite data into useful meteorological parameters. Techniques using microwave radiometric data, because of the transparency of clouds in the microwave region and because of the ability of microwave radiometers to sense a number of surface and atmospheric parameters, seem to the author to hold great promise. It is hoped that research into the use of satellite data will continue so that the promise may become fact.

REFERENCES

Arnold, C. P., 1977: Tropical cyclone cloud and intensity relationships. Atmos. Sci. Pap. 277, Colorado State University, Ft. Collins, Colorado, 154 pp.

Bates, J., 1977: Vertical shear of the horizontal wind speed in tropical cyclones. NOAA Tech. Memo. ERL WMPO-39, Miami, 19 pp.

Battan, L. J., 1973: Radar Observation of the Atmosphere. University of Chicago Press, Chicago, pp. 64-83.

Chandrasekhar, S., 1960: Radiative Transfer. Dover Publications Inc., New York, 393 pp.

Chapman, S. and J. Bartels, 1962: Geomagnatism, 2nd edition, Oxford University Press, London, p. 101.

Deirmendjian, D., 1963: Complete microwave scattering and extinction properties of polydispersed cloud and rain elements. Rand Corp. Rep. 12-422-PR, Santa Monica, Calibornia, 54 pp.

Dvorak, V. F., 1975: Tropical cyclone intensity analysis and forecasting from satellite imagery. Mon. Wea. Rev., 103, 420-430.

Fett, R. W., 1966: Upper-level structure of the formative tropical cyclone. Mon. Wea. Rev., 94, 9-18.

Fletcher, N., 1963: The Physics of Rainclouds. Cambridge University Press, Cambridge, 390 pp.

Frank, W. M., 1977: The structure and energetics of the tropical cyclone I. Storm structure. Mon. Wea. Rev., 105, 1119-1135.

Fritz, S., D. Q. Wark, H. E. Fleming, W. L. Smith, H. Jacobowitz, D. T. Hilleary, and J. C. Alishouse, 1972: Temperature sounding from satellites. NOAA Tech. Rep. NESS 59, 49 pp.

Fritz, S., L. F. Hubert, and A. Timchalk, 1966: Some inferences from satellite pictures of tropical disturbances. Mon. Wea. Rev., 94, 231-236.

Gaby, D. C., J. B. Lushine, B. M. Mayfield, S. C. Pearce, K. O. Poteat, and F. E. Torres, 1977: Atlantic tropical and subtropical cyclone classifications for 1976. NOAA Tech. Memo. NESS 87, 13 pp. (NTIS PB 269 G74/8GI).

Goody, R. M., 1964: Atmospheric Radiation I. Theoretical Basis. Oxford University Press, London, 436 pp.

Gray, W. M., 1977: Cyclone intensity determination through upper tropospheric reconnaissance. Postprints 11th Tech. Conf. Hurricanes and Tropical Meteorology, Miami, 288-293.

Gray, W. M. and D. J. Shea, 1973: The hurricane's inner core region. II. Thermal stability and dynamic characteristics. J. Atmos. Sci., 30, 1565-1576.

Gray, W. M. and D. J. Shea, 1976: Data summary of NOAA's hurricane inner-core radial leg flight penetrations 1957-1967, and 1969. Atmos. Sci. Pap. 257, Colorado State University, Ft. Collins, Colorado, 219 pp.

Hawkins, H. F. and D. T. Rubsam, 1968: Hurricane Hilda, 1964 II. Structure and budgets of the hurricane on October 1, 1964. Mon. Wea. Rev., 96, 617-636.

Hawkins, H. F. and S. M. Imbembo, 1976: The structure of a small intense hurricane--Inez, 1966. Mon. Wea. Rev., 104, 418-442.

Hebert, P. J. and Staff, NHC, 1977: Annual data and verification tabulation Atlantic tropical cyclones 1975. NOAA Tech. Memo. NWS NHC 2, Miami, 63 pp.

Herzberg, G., 1950: Molecular Spectra and Molecular Structure. I. Spectra of Diatomic Molecules, Second edition. D. Van Nostrand Co., Princeton, New Jersey.

Holton, J. R., 1972: An Introduction to Dynamic Meteorology. Academic Press, New York, 319 pp.

Hughes, L. A., 1952: On the low level wind structure of tropical cyclones. J. Meteor., 9, 422-428.

International Association of Meteorology and Atmospheric Physics (IAMAP) Radiation Commission, 1978: Terminology and units of radiation quantities and measurements, Boulder, 17 pp.

Jelesnianski, C. P., and A. D. Taylor, 1973: A preliminary view of storm surges before and after storm modifications. NOAA Tech. Memo. ERL WMPO-3, 33 pp.

Kidder, S. Q., 1976: Tropical oceanic precipitation frequency from Nimbus 5 microwave data. Atmos. Sci. Pap. 248, Colorado State University, Ft. Collins, Colorado, 50 pp.

Kidder, S. Q., W. M. Gray, and T. H. Vonder Haar, 1978: Estimating tropical cyclone central pressure and outer winds from satellite microwave data. Mon. Wea. Rev., 106, 1458-1464.

LaSeur, N. E. and H. F. Hawkins, 1963: An analysis of Hurricane Cleo (1958) based on data from research reconnaissance aircraft. Mon. Wea. Rev., 91, 694-709.

Liebe, H. J., G. G. Gimmestad, and J. D. Hopponen, 1977: Atmospheric oxygen microwave spectrum-experiment versus theory. IEEE Trans. Antennas Propagation, AP-25, 327-335.

Liebe, H. J. and G. G. Gimmestad, 1978: Calculation of clear air EHF refractivity. Radio Science, 13, 245-251.

Malkus, J. S. and H. Riehl, 1959: On the dynamics and energy transformations in steady-state hurricanes. National Hurricane Research Project Rep. No. 31, Dept. of Commerce, Washington, D. C., 31 pp.

NASA, 1976: Spacelab User's Guide. Available from the U.S. Government Printing Office, Washington, D. C., 20 pp.

Nordberg, W., J. Conaway, D. B. Ross, and T. Wilheit, 1971: Measurements of microwave emission from a foam-covered, wind-driven sea. J. Atmos. Sci., 28, 429-435.

Núñez, E. and W. M. Gray, 1977: A comparison between West Indies hurricanes and Pacific typhoons. Postprints 11th Tech. Conf. Hurricanes and Tropical Meteorology, Miami, 528-534.

Rodgers, E., R. C. Gentry, W. E. Shank, and V. Oliver, 1977: The benefits of using short interval satellite imagery to derive winds for tropical cyclones. Postprints 11th Tech. Conf. Hurricanes and Tropical Meteorology, Miami, 653-660.

Riehl, H., 1954: Tropical Meteorology. McGraw-Hill, 392 pp.

Riehl, H., 1963: Some relations between wind and thermal structure of steady-state hurricanes. J. Atmos. Sci., 20, 276-287.

Rosenkranz, P. W., D. H. Staelin, and N. C. Grody, 1978: Typhoon June (1975) viewed by a scanning microwave spectrometer. J. Geophys. Res., 83, 1857-1868.

Rosenkranz, P. W., 1975: Shape of the 5 mm oxygen band in the atmosphere. IEEE Trans. Antennas Propagation, AP-23, 498-506.

Rosenkranz, P. W. and D. H. Staelin, 1976: Summary of operations: The scanning microwave spectrometer (SCAMS) experiment. The Nimbus 6 Data Catalog, Vol. 3, NASA/Goddard Space Flight Center, Greenbelt, Maryland, pp. 1-2 through 1-4.

Sadler, J. C., 1964: Tropical cyclones of the Eastern North Pacific as revealed by TIROS observations. J. Appl. Meteor., 3, 347-366.

Savage, R. C., 1976: The transfer of thermal microwaves through hydrometeors. Ph.D. dissertation, University of Wisconsin-Madison, 147 pp.

Staelin, D. H., A. L. Cassel, K. F. Kunzi, R. L. Pettyjohn, R. K. L. Poon, and P. W. Rosenkranz, 1975: Microwave atmospheric temperature sounding: Effects of clouds on the Nimbus 5 satellite data. J. Atmos. Sci., 32, 1970-1976.

Staff, Joint Typhoon Warning Center, 1975: 1975 Annual Typhoon Report. Joint Typhoon Warning Center, COMNAVMARIANAS Box 12, FPO, San Francisco, 75 pp.

Staff, Joint Typhoon Warning Center, 1976: Tropical cyclone center fix data for the 1975 typhoon season. FLEWEACEN Tech. Note JTWC 76-5, Joint Typhoon Warning Center, COMNAVMARIANAS Box 12, FPO, San Francisco, 35 pp.

Stogryn, A., 1971: Equations for calculating the dielectric constant of saline water. IEEE Trans. Microwave Theory Technique, MTT-19, 733-736.

Stogryn, A., 1967: The apparent temperature of the sea at microwave frequencies. IEEE Trans. Antennas Propagation, AP-15, 278-286.

U. S. Standard Atmosphere Supplements, 1966: Available from the U.S. Government Printing Office, 289 pp.

Van Vleck, J. H., 1947a: Absorption of microwaves by water vapor. Phys. Rev., 71, 425-433.

Van Vleck, J. H., 1947b: Absorption of microwaves by oxygen. Phys. Rev., 71, 413-424.

Waters, J. W., K. F. Kunzi, R. L. Pettyjohn, R. K. L. Poons, and D. H. Staelin, 1975: Remote sensing of atmospheric temperature profiles with the Nimbus 5 microwave spectrometer. J. Atmos. Sci., 32, 1953-1969.

Westwater, E. R., 1972: Microwave emission from clouds. NOAA Tech. Rep. 219-WPL 18, Boulder, 43 pp.

Wilheit, T. T., 1972: The electrically scanning microwave radiometer (ESMR) experiment. The Nimbus 5 User's Guide, R. R. Sabatini, Ed., ERTS/Nimbus Project, NASA/Goddard Space Flight Center, Greenbelt, Maryland, 59-105.

APPENDIX I

MEAN ENVIRONMENT AND TEMPERATURE ANOMALIES OF TROPICAL CYCLONES (AFTER NÚÑEZ and GRAY, 1977)

WEST INDIES

MEAN TROPICAL CYCLONE ENVIRONMENT

PRESSURE	TEMPERATURE(°C)		MIXING RATIO (g kg^{-1})	
(kPa)	Mean	Std Err	Mean	Std Err
5.0	-59.73	.083		
7.0	-66.19	.092		
8.0	-69.29	.112		
10.0	-73.34	.123		
12.5	-72.12	.099		
15.0	-66.86	.075		
17.5	-60.46	.058		
20.0	-54.26	.056		
25.0	-42.78	.061		
30.0	-32.88	.064	.24	.005
35.0	-24.50	.063	.47	.011
40.0	-17.70	.057	.80	.020
50.0	- 6.71	.053	1.69	.038
60.0	1.63	.050	3.13	.058
70.0	8.66	.050	5.07	.074
80.0	14.43	.059	8.14	.087
85.0	17.08	.062	10.10	.084
90.0	19.86	.062	12.31	.077
95.0	22.77	.065	14.74	.086
100.0	25.75	.080	16.84	.088
101.3	26.13	.099	17.16	.105

WEST PACIFIC

MEAN TROPICAL CYCLONE ENVIRONMENT

PRESSURE (kPa)	TEMPERATURE (°C) Mean	Std Err	MIXING RATIO (g kg^{-1}) Mean	std Err
5.0	-61.61	.115		
7.0	-69.13	.151		
8.0	-73.80	.204		
10.0	-75.86	.156		
12.5	-72.43	.125		
15.0	-65.80	.095		
17.5	-58.84	.079		
20.0	-52.23	.068		
25.0	-40.45	.062		
30.0	-30.73	.066	.35	.009
35.0	-22.59	.085	.70	.036
40.0	-15.78	.071	1.09	.025
50.0	- 5.28	.067	2.26	.045
60.0	2.88	.068	3.80	.065
70.0	9.74	.072	5.56	.086
80.0	14.89	.086	8.75	.099
85.0	17.36	.084	10.56	.102
90.0	19.98	.081	12.48	.104
95.0	23.12	.071	14.88	.114
100.0	25.96	.118	17.34	.146
101.3	25.99	.087	17.54	.111

WEST INDIES HURRICANE TEMPERATURE ANOMALIES (K)

PRESSURE (kPa)	0°-1°	1°-2°	2°-3°	3°-4°	4°-5°	5°-6°	6°-7°	7°-9°	9°-11°	11°-13°	13°-15°
5.0	1.63*	-.45*	-1.22	-.78	-.71	-.18*	-.09*	-.11*	.11*	.28	.29
7.0	-.26*	-1.37	-1.22	-1.15	-.40	-.48	-.26*	-.05*	.26	.53	.87
8.0	-1.21	-2.18	-1.65	-1.67	-.87	-1.00	-.39	-.28	.30	.67	1.10
10.0	-2.41*	-2.03	-2.55	-2.13	-2.07	-1.75	-1.02	-.66	.27	.88	1.33
12.5	-2.98	-1.96	-2.09	-1.81	-1.79	-1.20	-1.17	-.66	.09*	.77	1.07
15.0	-1.05*	-.27*	-.76	-.35	-.47	-.26	-.28	-.11*	.17	.48	.55
17.5	1.33	.74	.53	.42	.29	.35	.23	.19	.17	.14	-.06*
20.0	2.57	1.66	1.42	1.12	.86	.83	.58	.48	.07*	-.19	-.45
25.0	4.11	2.64	2.23	1.80	1.49	1.20	.88	.54	-.02*	-.50	-.76
30.0	4.31	2.85	2.38	1.95	1.59	1.07	.79	.46	-.11*	-.59	-.90
35.0	3.82	2.77	2.04	1.70	1.24	.99	.64	.37	-.14	-.63	-.93
40.0	4.08	2.51	1.80	1.43	1.11	.87	.54	.34	-.05*	-.62	-.86
50.0	3.09	1.66	1.20	1.01	.73	.64	.29	.02*	-.10*	-.59	-.80
60.0	1.25	.52	.44	.50	.49	.42	.20	.15	-.06*	-.46	-.66
70.0	.93*	-.15*	.12*	.33	.37	.35	.10*	.11*	-.05*	-.45	-.64
80.0	.17*	-.14*	.10*	.24	.25	.27	.16*	.12*	-.12	-.50	-.76
85.0	-.52*	-.15*	.14*	.39	.26	.18	.13*	.12*	-.22	-.57	-.90
90.0	-.90*	-.24*	.14*	.37	.29	.21	.07*	.01*	-.28	-.68	-.96
95.0	-.97*	-.17*	.19*	.29	.36	.19	.01*	-.15*	-.36	-.81	-1.05
100.0	-2.28	-.46	-.02*	.22*	.39	.12*	-.16*	-.24	-.37	-1.05	-1.23
101.3	-1.37	-.57	-.20*	.25*	.50	.09*	-.04*	-.19*	-.33	-1.17	-1.44

*Not statistically significant at the 5% level.

WEST PACIFIC
TYPHOON TEMPERATURE ANOMALIES (K)

PRESSURE	0°-1°	1°-2°	2°-3°	3°-4°	4°-5°	5°-6°	6°-7°	7°-9°	9°-11°	11°-13°	13°-15°
5.0	- .94*	-.31*	.27*	-.09*	.10*	-.17*	-.15*	.23*	.36	.55	.42
7.0	- .90*	.36*	.92	.63	.57	1.50	.96	1.24	1.49	1.73	1.91
8.0	-3.40*	.69*	.04*	-.34*	.03*	.03*	-.02*	.35*	.88	1.42	1.47
10.0	-1.81*	.81*	-.81	.01*	-.55	.62*	.63	1.02	1.63	2.04	2.67
12.5	2.94	1.75*	.14*	.33*	-.11*	.70	.90	1.15	1.61	1.96	2.13
15.0	3.88	2.15	1.07	1.09	.62	.82	1.10	1.10	1.24	1.34	1.27
17.5	4.68	3.15	1.83	1.65	1.17	1.02	1.20	1.01	.95	.82	.66
20.0	5.26	3.51	2.45	1.95	1.43	1.22	1.23	.86	.68	.44	.19
25.0	6.25	4.10	2.98	2.38	1.91	1.43	1.15	.87	.48	.03*	-.38
30.0	5.99	3.92	3.04	2.49	2.10	1.54	1.34	.89	.28	-.21	-.64
35.0	5.11	3.63	2.84	2.28	1.85	1.25	1.10	.63	.04*	-.42	-.87
40.0	4.46	3.21	2.40	1.92	1.33	1.04	.72	.34	-.12	-.59	-1.05
50.0	2.89	2.22	1.64	1.37	1.04	.67	.44	.14	-.23	-.79	-1.17
60.0	1.91	1.37	.99	.81	.66	.45	.27	.12	-.28	-.78	-1.25
70.0	1.32	1.03	.85	.84	.71	.50	.27	.23	-.24	-.76	-1.30
80.0	1.63	1.20	1.11	1.14	1.05	.79	.33	.33	-.17	-.76	-1.28
85.0	1.36	1.13	1.07	1.11	.99	.68	.29	.11*	-.32	-.90	-1.40
90.0	.89	.98	.86	.86	.76	.43	.01*	-.07*	-.54	-1.06	-1.60
95.0	-.27*	.29*	.43	.60	.60	.29	.03*	.14*	-.29	-.54	-.71
100.0	.54*	-.01*	.60	.84	.55	.28*	-.42*	-.44	-1.01	-1.64	-2.16
101.3	-1.53	-.38	-.16*	.17*	.22*	-.26*	-.52	-.49	-.90	-1.37	-1.92

*Not statistically significant at the 5% level.

APPENDIX II

ON HYDROSTATIC BALANCE IN TROPICAL CYCLONES

The hydrostatic approximation may be shown to be valid in tropical cyclones by scale analysis _a la_ Holton (1972). The vertical momentum equation is

$$\frac{dw}{dt} - 2\Omega u\cos\phi - \frac{u^2+v^2}{a} = -\frac{1}{\rho}\frac{\partial p}{\partial z} - g \ , \tag{A1}$$

where w is vertical velocity, u and v are horizontal velocities, Ω is the angular velocity of the earth, a is the radius of the earth, ρ is density, p is pressure, g is gravity, ϕ is latitude, z is height and t is time. If it can be shown that the two terms on the right in Eq. (A1) dominate, then the hydrostatic equation is valid. Table A1 shows the scales used in this analysis.

Because the horizontal pressure gradient is necessary to analyze the right hand side of Eq. (41), it will be analyzed separately. Defining the horizontally averaged pressure as $p_o(z)$ and $\rho_o(z)$ as the standard density which is exactly in hydrostatic equilibrium with $p_o(z)$,

$$\rho_o(z) \equiv -\frac{1}{g}\frac{d\,p_o}{dz} \ , \tag{A2}$$

the pressure and density may be written

$$p(x,y,z,t) = p_o(z) + p'(x,y,z,t) \tag{A3}$$

$$\rho(x,y,z,t) = \rho_o(z) + \rho'(x,y,z,t) \tag{A4}$$

Assuming that ρ'/ρ_o and p'/p_o are much less than one, the right hand side of Eq. (A1) may be approximated as follows

Table A1

Scales Used for Analyzing Eq. (A1).

SCALE	SYMBOL	VALUE
Horizontal Velocity	U	50 $m\,s^{-1}$
Horizontal Length	L	100 km
Vertical Velocity	W	0.1 $m\,s^{-1}$
Depth	H	10 km
Angular Velocity	Ω	$10^{-4}\ s^{-1}$
Radius of Earth	a	10^{7} m
Density	ρ_o	1 $kg\ m^{-3}$
Gravity	g	10 $m\,s^{-2}$
Surface Pressure	p_o	100 kPa
Horizontal Pressure Variation	p'	3 kPa
Horizontal Density Variation	ρ'	0.03 $kg\ m^{-3}$

$$-\frac{1}{\rho}\frac{\partial p}{\partial z} - g = \frac{1}{(\rho_o + \rho')}\frac{\partial}{\partial z}(p_o + p') - g$$

$$\simeq \frac{1}{\rho_o}\left[\frac{\rho'}{\rho_o}\frac{d\, p_o}{dz} - \frac{\partial p'}{\partial z}\right]$$

$$= -\frac{1}{\rho_o}\left[\rho' g + \frac{\partial p'}{\partial z}\right]. \qquad \text{(A5)}$$

The scale for p' may be obtained by assuming the wind is in gradient balance

$$\frac{v^2}{r} + 2\Omega \sin\phi v = \frac{1}{\rho}\frac{\partial p}{\partial r} \simeq \frac{1}{\rho_o}\frac{p'}{L} \qquad \text{(A6)}$$

For $v = 50$ m s^{-1} and $r = 100$ km (outside the radius of maximum wind) $p' \approx 3$ kPa. At low levels in a tropical cyclone the temperature anomaly is small. Therefore,

$$\rho' \approx \frac{p'}{RT} = \rho_o \frac{p'}{p_o} = 0.03 \text{ kg m}^{-3} \qquad \text{(A7)}$$

Inserting these results into Eq. (A5) gives

$$\frac{\rho'}{\rho_o} g \approx 0.3 \text{ m s}^{-2} ; \qquad \text{(A8)}$$

$$\rho_o \frac{\partial p'}{\partial z} \approx \rho_o \frac{p'}{H} = 0.3 \text{ m s}^{-2} \qquad \text{(A9)}$$

The right hand side of Eq. (A1) is approximately 0.3 m s^{-2}. The entire equation may now be scaled as in Table A2.

Clearly the right hand side dominates, and the hydrostatic approximation is valid. One can repeat the calculation at length scales of 10 km and find that the hydrostatic approximation is still relatively good. For smaller scales, however, it breaks down.

Table A2

Scale Analysis of Eq. (A1)

MOMENTUM EQ.	$\frac{dw}{dt}$	$2\Omega u \cos\phi$	$\frac{u^2 + v^2}{a}$	$= -\frac{1}{\rho}\frac{\partial p}{\partial z} - g$
SCALES	$\frac{HW}{L}$	ΩU	$\frac{U^2}{a}$	(see above)
MAGNITUDES ($m\ s^{-2}$)	5×10^{-5}	5×10^{-3}	3×10^{-4}	0.3

BIBLIOGRAPHIC DATA SHEET	1. Report No. CSU-ATSP-307	2.	3. Recipient's Accession No.
4. Title and Subtitle Determination of Tropical Cyclone Surface Pressure and Winds from Satellite Microwave Data			5. Report Date April, 1979 6.
7. Author(s) Stanley Q. Kidder			8. Performing Organization Rept. No. 307
9. Performing Organization Name and Address Department of Atmospheric Science Colorado State University Fort Collins, Colorado 80523			10. Project/Task/Work Unit No. 11. Contract/Grant No. NASA NSG-5258
12. Sponsoring Organization Name and Address National Aeronautics and Space Administration Goddard Space Flight Center Greenbelt, MD 20771			13. Type of Report & Period Covered 14.

15. Supplementary Notes

16. Abstracts

Upper tropospheric temperature anomalies above tropical cyclones are detected in data from the 55.45 GHz channel of the Nimbus 6 Scanning Microwave Spectrometer (SCAMS). Brightness temperature gradients are related to gradients in the logarithm of surface pressure through the hydrostatic and radiative transfer equations. The derived surface pressure gradients are then related to surface wind speeds through the gradient wind equation. The technique, called the Surface Wind Inference from Microwave data (SWIM) technique, is first tested using simulated satellite data constructed from temperature, pressure and height data recorded by reconnaissance aircraft in four hurricanes. Wind speeds in the 80-95 kPa region are estimated with 2-3 ms^{-1} accuracy. Next, data from the SCAMS 55.45 GH channel over eight typhoons during 1975 are used to estimate the radii of 30 kt and 50 kt winds. Accuracies of $\pm$80 km and $\pm$65 km are found. It is suggested that the technique be further tested using data from the 54.96 GHz channel of the TIROS-N Microwave Sounding Unit (MSU).

17. Key Words and Document Analysis. 17a. Descriptors

Microwave Sounder
Satellite
Tropical Cyclone
Outer Surface Wind Speeds
Surface Pressure Gradients

17b. Identifiers/Open-Ended Terms

17c. COSATI Field/Group

18. Availability Statement	19. Security Class (This Report) UNCLASSIFIED	21. No. of Pages 102
	20. Security Class (This Page UNCLASSIFIED	22. Price